LBNL-47177
Preprint

ERNEST ORLANDO LAWRENCE
BERKELEY NATIONAL LABORATORY

The Photodissociation Dynamics of Cyclic Sulfides Probed with Tunable Undulator Radiation

Arthur G. Suits and Fei Qi

Chemical Sciences Division

November 2000

Invited Review for
Journal of Electron Spectroscopy and Related Phenomena

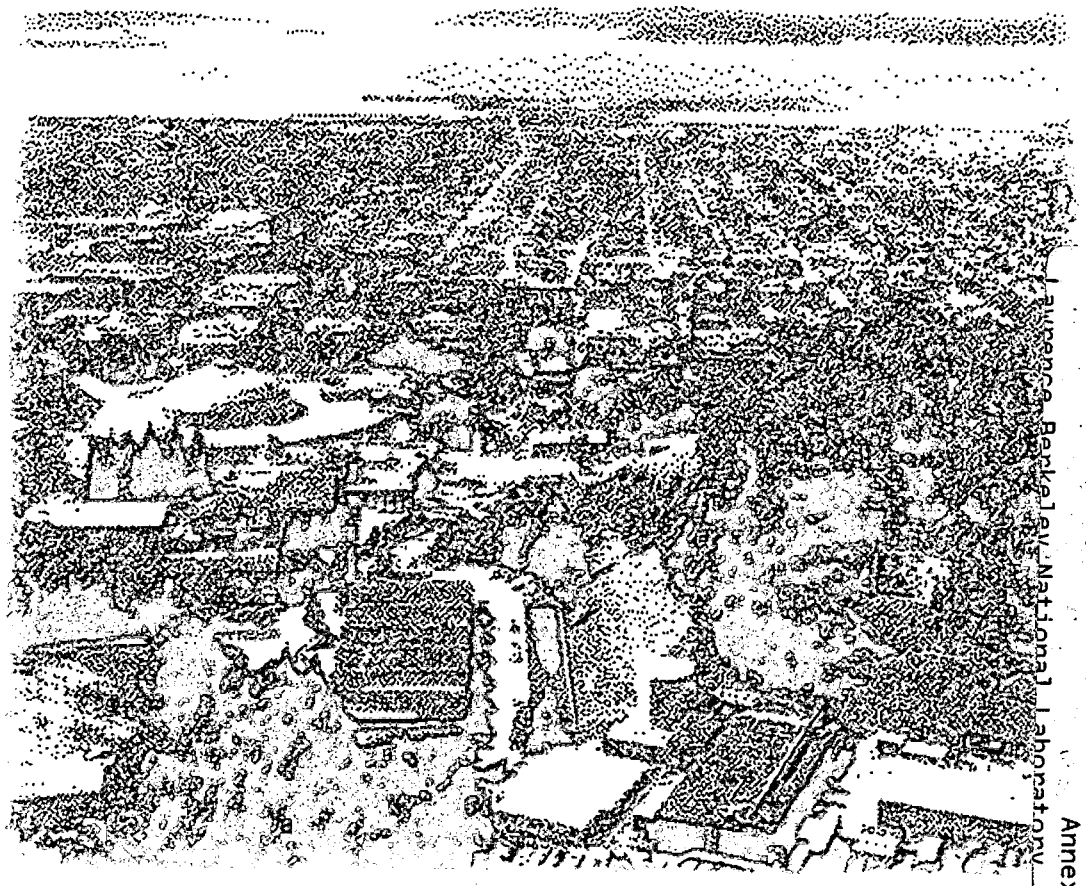

DISCLAIMER

LBNL-47177

The Photodissociation Dynamics of Cyclic Sulfides Probed with Tunable Undulator Radiation

Arthur G. Suits and Fei Qi

Chemical Sciences Division
Ernest Orlando Lawrence Berkeley National Laboratory
University of California
Berkeley, California 94720

November 2000

This work was supported by the Director, Office of Science, Office of Basic Energy Sciences, Chemical Sciences Division, of the U.S. Department of Energy under Contract No. DE-AC03-76SF00098.

The Photodissociation Dynamics of Cyclic Sulfides Probed with Tunable Undulator Radiation

Arthur G. Suits*

Department of Chemistry, State University of New York at Stony Brook, Stony Brook, NY 11794, and Chemistry Department, Brookhaven National Laboratory, Upton, NY 11973

Fei Qi

Chemical Sciences Division, Ernest Orlando Lawrence Berkeley National Laboratory, Berkeley, CA 94720

Abstract

The combination of tunable synchrotron radiation with photofragment translational spectroscopy has been used to probe the photodissociation dynamics of a variety of cyclic sulfides. The results demonstrate the many advantages using synchrotron radiation in place of electron impact ionization in photochemistry studies. Our *universal* and *selective* experimental approach is easily able to distinguish the ground state $S(^3P)$ and the first excited state $S(^1D)$, for example, and provides photoion yield spectra of all products. These measurements afford unambiguous identification of the primary decay pathways, as well as unique insights into the properties of the product species, often radicals or transient metastable species.

* To whom correspondence should be addressed. E-mail: asuits@mail.chem.sunysb.edu

1. Introduction

The pioneering work of Busch and Wilson [1-3] established the technique of crossed-laser and molecular-beam photofragment translational spectroscopy (PTS) with time-of-flight (TOF) mass-spectrometric detection as a universal method for investigating photodissociation dynamics. The study of photodissociation dynamics has grown explosively in the past few decades. Recent advances on this field have been described in several review papers.[4-7] The PTS method is a very powerful tool with which to understand elementary photodissociation dynamics. In most cases PTS experiments employ electron impact (EI) ionization as product detection. Although a great many important results have been achieved with the use of EI, several shortcomings of EI based experiments have long been recognized. These include: dissociative ionization of larger neutral products into smaller fragments, appearing at different mass-to-charge ratios, resulting in ambiguous and uncertain interpretation; large inherent backgrounds at certain masses; and the possibility for many different molecules or isomers to give signals at the same mass-to-charge ratio. State-resolved laser probing overcomes some of these difficulties, providing the ability to study dissociation dynamics in great detail. However, these approaches are are not well-suited to studying the global dynamics of molecules; their use is limited to smaller systems whose spectroscopy is well known. In the following pages we intend to show that the use of PTS with intense, tunable synchrotron radiation simultaneously enjoys the advantages of state-resolved laser probing of photoproducts with those of universal mass-spectrometric based probes.

The use of tunable VUV light as the ionization source in TOF measurements has the following tremendous advantages over the widely used electron bombardment ionization method [8-10]. Tunable VUV ionization can (1) be selective since different molecules can have different ionization potentials, (2) allow for the determination of the relationship between internal energy and ionization cross section, and (3) allow more straightforward detection and analysis of multiple channel processes. Finally, since undulator VUV light is focusable, the ionization region can be much smaller than a comparable electron

bombardment ionizer, making both the TOF spectra and angular resolution much higher and background contribution lower.

This paper will describe some new results for 193 nm photodissociation of some cyclic sulfides: ethylene sulfide (C_2H_4S), propylene sulfide (C_3H_6S), thietane (C_3H_6S), and thiophene (C_4H_4S), with the tunable synchrotron radiation as probe light source from the Advanced Light Source of Lawrence Berkeley National Laboratory.

2. Experimental Method

The experiments were performed on Chemical Dynamics Beamline 9.0.2.1 of the Advanced Light Source using a rotatable source molecular beam apparatus described in detail elsewhere.[11] Helium was bubbled through samples cooled to yield 10% beams at a total pressure of 800 Torr. The appropriate mixture was fed through a pulsed valve into a source chamber at $5x10^{-4}$ Torr or so. The nozzle of the valve was heated to avoid cluster formation. The resulting molecular beam was collimated with two skimmers. The molecular beam velocity and speed ratio were measured accomplished via the hole-burning technique at the parent ion mass. The beam parameters were determined by fitting laser-induced depletion profiles and assuming a number density distribution $f(v) \propto v^2 e^{-((v/\alpha)-S)^2}$ [12-14].

The molecular beam was intersected at 90° with an ArF excimer laser beam. The laser beam was focused to a spot of size 2×4 mm^2 and aligned perpendicular to the plane containing the molecular beam and detector axes, on the axis of rotation of the molecular beam source. Photofragments entering the triply differentially pumped detector region were photoionized 15.2 cm downstream from the interaction region using tunable synchrotron radiation. The characteristics of the light source have been discussed in detail elsewhere,[15] which includes a flux of 10^{16} photons/sec (quasi-continuous), an energy bandwidth of 2.2%, and a cross section in the probe region of 0.1×0.2 mm^2. The photoionized products were mass selected by a quadrupole mass filter and the ions were counted with a Daly ion counter. Time-of-flight spectra of the neutral products were measured with a multichannel scaler (MCS). Timing sequences for the laser, pulsed valve, and the MCS were controlled using a digital delay generator. Laser power

dependence was measured for all observed channels. Care was taken to ensure that the TOF data were free of multiphoton effects.

The tunability of the VUV light source allowed for the measurements of photoionization efficiency (PIE) spectra and for the selective ionization of products with very low background counts. A series of TOF spectra were recorded at a fixed angle for different photoionization energies, then normalized for the probe photon flux, and integrated to obtain the PIE spectra. A gas harmonic filter filled with about 25 Torr Ar was used to eliminate higher harmonics of the undulator radiation.[16] A MgF_2 optical filter was also used to eliminate small contamination of the probe light by higher energy photons when the probing energy was below 11.0 eV.

In all the TOF spectra presented here, the open circles represent the experimental data; the dash lines, the dash-dot lines, and the dot lines are single channel contributions to the forward convolution fit, and the solid lines are the overall fit to the data. A forward convolution fit to data was used to get total center-of-mass translational distributions, $P(E_T)$ [17].

3. Results

Photoabsorption spectra of ethylene sulfide and propylene sulfide show a series of sharp resonance peaks beginning at 192.2 nm[18], which is close to the spectral output (193 nm) of an ArF excimer laser. These peaks have been assigned as a vibrational progression in the 4p Rydberg transition[19]. Figure 1 shows the absorption spectra of ethylene sulfide, propylene sulfide, and thietane. In this paper, we focus on our results on the S + C_nH_m channels from 193 nm photodissociation of ethylene sulfide, propylene sulfide, thietane, and thiophene, although multi-channels were observed in our studies.

The ionization potential (IP) of the sulfur atom are well known to be 10.36 eV and 9.21 eV for the ground state (^3P) and the first excited state (^1D), respectively[20]. Thus, in this study the S(^1D) atom can be selectively ionized by using tunable VUV light at 9.5 eV, whereas contributions from both S(^3P) and S(^1D) can arise at energy of 10.8 eV. Figure 2 shows a schematic energy diagram of neutral sulfur atom and its ion.

3.1 Ethylene Sulfide

Ethylene sulfide (C_2H_4S) is a three-membered cyclic molecule. Felder and coworker observed three primary dissociation channels ($S(^1D) + C_2H_4$, $HS + C_2H_3$, and $H + C_2H_3S$) from 193 nm photodissociation of this species using the PTS method, but with electron impact ionization [21]. The translational energy distribution beyond the available energy for the $S(^1D) + C_2H_4$ channel was assigned to the $S(^3P) + C_2H_4$ products in Felder et al.'s study[21]. A Doppler broadened laser induced florescence probe employed in Kim et al.'s study was specific to nascent S atoms and thus to the dissociation process yielding $S + C_2H_4$[22]. They probed for the three lowest electronic states of sulfur atoms, $S(^3P)$, $S(^1D)$, and $S(^1S)$, but found evidence only for the formation of sulfur in the ^1D state.

Results for ethylene sulfide at 193 nm photodissociation obtained on the Chemical Dynamics Beamline show six primary dissociation channels shown as the following:

$$C_2H_4 + h\nu_{193nm} \rightarrow S(^1D) + C_2H_4(^1A_g) \qquad \Delta H_{rxn} = -65 \text{ kcal/mol} \qquad (1)$$

$$C_2H_4 + h\nu_{193nm} \rightarrow S(^3P) + C_2H_4(^1A_g) \qquad \Delta H_{rxn} = -92 \text{ kcal/mol} \qquad (2)$$

$$C_2H_4 + h\nu_{193nm} \rightarrow S(^3P) + C_2H_4(^3B_{1u}) \qquad \Delta H_{rxn} = -28 \text{ kcal/mol} \qquad (3)$$

$$C_2H_4 + h\nu_{193nm} \rightarrow HS + C_2H_3 \qquad \Delta H_{rxn} = -66 \text{ kcal/mol} \qquad (4)$$

$$C_2H_4 + h\nu_{193nm} \rightarrow H_2S + C_2H_2 \qquad \Delta H_{rxn} = -121 \text{ kcal/mol} \qquad (5)$$

$$C_2H_4 + h\nu_{193nm} \rightarrow H + C_2H_3S \qquad \Delta H_{rxn} \approx -43 \text{ kcal/mol} \qquad (6)$$

ΔH_{rxn} is the reaction energy. Here the heats of formation of c-C_2H_4S, $C_2H_4(^1A_g)$, $C_2H_4(^3B_{1u})$, $S(^3P)$, $S(^1D)$, H_2CCH, HS, H_2CC:, HCCH, H_2S, C_2H_3S and H are 22.4,[21] 12.54,[23] 76.5,[24] 66.2,[23] 92.7,[20] 71.5,[25] 33.3,[23] 100.3,[26] 54.5,[27] –4.9,[23] ~75,[21] and 52.1[23] kcal/mol, respectively. We will focus our results on the first three channels in this article.

3.1.A. TOF spectra of m/e = 32 (S).

Figure 3(a) and 3(b) show TOF spectra of m/e 32 (S) at the indicated scattering angles and 9.5 eV probe photon energy with a MgF_2 optical filter. Two peaks are readily apparent at 43 and 73 μsec in the TOF spectrum of Fig. 3(a). Less obvious, but nevertheless apparent is a shoulder at 52 μsec. Three translational energy distributions

(labeled **A**, **B**, and **C**), $P(E_T)$s, shown in Fig. 4(a) were used to fit the fast part (the dash line) , the middle part (the dash-dot line), and the slow part (the dot line) of the TOF spectra of Fig. 3(a and b), respectively. The average translational energy distribution is 42.8, 23.7, and 8.7 kcal/mol for the $P(E_T)_A$, the $P(E_T)_B$, and the $P(E_T)_C$, respectively. The maximum translational energy in each distribution was derived to be 65, 34, and 24 kcal/mol, respectively for the three components mentioned above. In each case the available energy is 65 kcal/mol. We should keep in mind that the decomposition into the three $P(E_T)$s is somewhat arbitrary, but the overall sum of these $P(E_T)$s is not. These $P(E_T)$s correspond to a channel producing excited state sulfur (^1D) and ground state ethylene (^1A_g) (reaction **1**), because the photoionization energy used here is below the IP of the ground state sulfur. We assign each peak in Fig. 4a to dissociation on different potential energy surfaces. We will discuss the dissociation mechanism later.

The above measurements were repeated at 10.8 eV and the results are shown in Fig. 3(c and d). Three peaks are clearly observed in the TOF spectra at the scattering angle of 20°. At this probe energy, both excited $S(^1D)$ and ground $S(^3P)$ products contribute, but no S atom signal will arise from fragmentation of large species (C_2H_3S, H_2S, and HS), since the probe energy is below the onsets of dissociative ionization for any of the other fragments. The branching ratio of the three $P(E_T)$s shown in Fig. 4(a) should be constant in fitting the 10.8 eV TOF spectra of m/e 32. Therefore, the three $P(E_T)$s shown in Fig. 4(a) were combined to one $P(E_T)$, shown as the solid curve of Fig. 4(a), by using the known intensity and ratio. Two additional translational energy distributions shown in Fig. 4(b) and 4(c) were used to fit the 10.8 eV data very well.

The maximum translational energy of the distribution shown in Fig. 4(b) is 85 kcal/mol, which exceeds the available energy for the $S(^1D) + C_2H_4(^1A_g)$ (reaction **1**) and the $S(^3P) + C_2H_4(^3B_{1u})$ (reaction **3**) channels. However, it is very close to the available energy for the spin-forbidden $S(^3P) + C_2H_4(^1A_g)$ channel (reaction **2**). On the other hand, comparing the TOF spectra of mass 32 obtained below and above the IP of the ground state atom, the *second* peak (~52 μs) of the S atoms actually corresponds partly to the production of ground state sulfur atoms. These ground state (^3P) sulfur atoms are formed at energies near that anticipated for the production of the excited *triplet* state ($^3B_{1u}$) of ethylene (reaction **3**). This new channel including excited state triplet ethylene was not

identified in Felder et al.'s study employing electron impact ionization[21], where it could not have been recognized as a specific feature of the ground state S atom product. The corresponding translational energy distribution is shown in Fig. 4(c). Consequently, we assign the $P(E_T)$ of Fig. 4(c) corresponds to the $S(^3P) + C_2H_4(^3B_{1u})$ channel. The channel representing the production of $S(^3P)$ and $C_2H_4(^1A_g)$ has an average translational energy of 20 kcal/mol with an estimated exit barrier of 6.7 kcal/mol. If we look at the $P(E_T)$ of Fig. 4(b) in detail, it looks like two $P(E_T)$s overlap: one is very broad, another one very narrow with a peak at around 6.7 kcal/mol. This spin-forbidden dissociation could proceed via different mechanism on two surfaces. In addition, the maximum translational energy of the $S(^3P) + C_2H_4(^3B_{1u})$ channel is 34 kcal/mol with an average translational energy of 23.7 kcal/mol. The $P(E_T)$ of Fig. 4(c) indicates an exit barrier of roughly 24 kcal/mol for this channel.

3.1.B. TOF spectra of m/e = 28 (C_2H_4) and Triplet Ethylene

Fig. 5(a, b) show the TOF spectra of m/e = 28 (C_2H_4), the momentum matched partner of m/e 32, at the scattering angle of 20° with photon energies of 11.0 and 10.0 eV, respectively. The TOF spectra of m/e 28 were fitted very well using the $P(E_T)$s shown in Fig. 4(a, b, c), with some adjustment of their relative contributions, consistent with the anticipated dependence of the photoionization cross section on internal energy in the product. Indeed, we can get some insight into this by examining the behavior of the TOF spectra as a function of probe photon energy. The ionization potential of ethylene is well known to be 10.51 eV[27]. Comparing the TOF spectra of m/e 28 recorded above and below the IP of C_2H_4, an evident change occurred in the fast part. This means the "cold" ethylene cannot be ionized at the photon energy of 10.0 eV. The second peak becomes clearer, which confirms the presence of considerable internal energy.

The heat of formation for triplet ethylene could be derived from the translational energy distribution of figure 4(c), assuming the dissociation for $S(^3P) + C_2H_4(^3B_{1u})$ occurs on the excited state potential energy surface. The heat of formation for triplet ethylene was derived to be 70 ± 3 kcal/mol, which is 58 kcal/mol above the ground state. Our experimental result is little different from the theoretical predictions: the ground state of ethylene is more stable than the triplet state by 46,[28] and 64 kcal/mol[24] at their

potential energy minima located at twisting angles of 0° (^1A_g), and of 90° ($^3B_{1u}$). Electron energy loss spectroscopy and theoretical calculation revealed that the $1^1A_g \rightarrow 1^3B_{1u}$ vertical transition energy occurred at 97 kcal/mol[29] and 106 kcal/mol,[24] respectively.

3.1.C. Branching Ratio Measurements

Attempts were made to measure the relative branching ratio between processes **1**, **2**, and **3**. Branching ratio measurements near the ionization threshold can be misleading, however, since the ionization cross section, σ_i, for S(^{1}D) and S(^{3}P) can be different near their respective onsets and are often perturbed by strong autoionization resonances[30-32]. Previous measurements have shown the photoionization efficiency to be similar for the two states at probe energy of 15 eV[33]. Thus, measurements of TOF spectra of m/e 32 were made at 15.0 eV photoionization energy and are shown in Figs. 5(c) and 5(d). The three $P(E_T)$s in Fig. 4(a, b, c) fitted these TOF spectra very well. According to this fit, the branching ratio for **1**, **2**, and **3** is 41:57:2.

3.1.D. Dissociation Mechanism

Figure 6 shows an energy diagram with the roughly estimated reaction barriers for all observed dissociation channels from ethylene sulfide at 193 nm excitation. A detailed description was given in our previous paper in order to estimate the reaction barrier.[10]

Three translational energy distributions were used to fit the S(^{1}D) + C_2H_4(^1A_g) channel. The question, then, is the nature of the dynamics underlying these distinct distributions. The initially excited Rydberg state of c-C_2H_4S is expected to have predominantly singlet character,[19] and the products are all singlets, so for these channels we confine our discussion to the singlet surfaces. First, we discuss the formation mechanism associated with $P(E_T)_A$ of Fig. 4(a). Fig. 7 shows the singlet potential energy profiles for ethylene sulfide dissociation in C_{2v} symmetry as a function of the S-C_2H_4 distance, obtained using the time-dependent (TD) DFT method.[10] The dissociation corresponding to $P(E_T)_A$ is likely to occur directly on the initially excited $^1A_1$ state, giving rise to the greatest translational energy release. Furthermore, another dissociation process, corresponding to $P(E_T)_B$, is likely to start with the excited $^1A_1$ state, then dissociation occurs after internal conversion to the $^1B_2$ surface. Although this coupling

vanishes in a strict C_{2v} symmetry, in the C_s symmetry space in which the dissociation actually occurs, this coupling can be significant. This pathway gives a calculated heat of reaction equal to 95.4 kcal/mol, whereas, the experimental heat of reaction is 83 kcal/mol for the $C_2H_4(^1A_g)$ + $S(^1D)$ channel. A possible source of the difference is that the singlet electronic state of the S atom described by the Gaussian-98 program[34] is a mixture of ^1D and ^1S, instead of a pure ^1D. Furthermore, it is not surprising that the calculated potential energy surfaces are higher than the experimental excitation energy of 148 kcal/mol (193 nm) because the calculated singlet potential profiles were derived by changing only one coordinate, the C-S distance, and maintaining the C_{2v} symmetry. In fact the excited states of c-C_2H_4S are ring distorted equilibrium conformations. Finally, the lowest energy peak in the $S(^1D)$ distribution is likely to arise from internal conversion from the aforementioned states to the ground state. The $^1B_1$ and $^1A_2$ surfaces shown in Figure 7 are not likely to play a role, since even in C_s symmetry, they become A″, so that coupling to A′ states is negligible. Imaging experiments show significant anisotropy in the $S(^1D)$ products, confirming this picture of rapid dissociation.[35]

The channel of $S(^3P)$ + $C_2H_4(^1A_g)$ is spin-forbidden. The occurrence of this spin-forbidden channel is not too surprising because the heavy S atom increases the probability of intersystem crossing. In fact, abundant formation of spin-forbidden fragment pairs has been observed from other sulfides such as CS_2 [36], SO_2 [37], and thiophene [38]. To dissociate into $S(^3P)$ and $C_2H_4(^1A_g)$, c-C_2H_4S must first undergo an intersystem crossing and ring-opening reaction to form biradical.[10] This biradical then forms the products $S(^3P)$ and $C_2H_4(^1A_g)$ via a transit structure. The G3 barrier of this stepwise reaction is 59.5 kcal/mol, in fair agreement with the experimental result (63±2 kcal/mol). This small exit barrier (1.5 kcal/mol, see Fig. 6) is also in good agreement with the previous report: a reaction barrier of ground-state sulfur atom with ethylene was measured to be 1.58 kcal/mol [39]. On the other hand, the other dissociation is likely to begin with excitation of the singlet $^1A_1$ state, followed by an intersystem crossing to the triplet state $^3B_2$. The complicated intersystem crossing is also reflected in the $P(E_T)$ of Fig. 4(b), in which the translation energy distribution beyond ~20 kcal/mol becomes flat.

Finally, we discuss the *triplet* ethylene channel. The production of $S(^3P)$ plus $C_2H_4(^3B_{1u})$ is also consistent with a process occurring on a singlet electronic surface. This

is a direct dissociation process occurring on the singlet excited potential energy surface without internal conversion. Hence, the triplet ethylene can be formed at near its equilibrium geometry, in which the two CH_2 groups are believed to lie in perpendicular planes. Thus we can derive an estimate, actually an upper limit, for the heat of formation for triplet ethylene. We should note that the assignment of the intermediate peak in the triplet S product to triplet ethylene is by no means definitive. Other possible explanations include internal conversion with dissociation on a different potential surface, as invoked for the $S(^1D)$ product. It might be tempting to associate this peak with a similar peak in the $S(^1D)$ distribution. A moment's consideration reveals, however, owing to the different electronic energy in the products, it cannot be related to the middle peak in the $S(^1D)$ distribution. We believe, in fact that this peak in the $S(^3P)$ distribution is related to the *fastest* peak in the $S(^1D)$ distribution, i.e., it arises from direct dissociation on the initially prepared singlet surface. Although the evidence presented here for the production of triplet ethylene from ethylene sulfide photodissociation is by no means definitive, we believe this is the most likely explanation for the observations. An indirect support for this assignment may be found in recent work on a related molecule, ethylene episulfoxide (C_2H_4SO), by Weiner and coworkers [40]. They used time-resolved laser-induced fluorescence spectroscopy to probe the SO ($X^3\Sigma^-$) photofragment on the ($B^3\Sigma^-$—$X^3\Sigma^-$) transition [40]. Two physical models, Franck-Condon and impulsive, were used to model the distribution of internal energy in the SO ($X^3\Sigma^-$) photofragment from 193 and 248 nm photodissociation of C_2H_4SO. Both models demonstrated that a reasonable fit to the experimental data was obtained only when the ethylene is triplet state ($^3B_{1u}$), not ground state. Furthermore, they suggested that the photodissociation of C_2H_4SO, at both 193 and 248 nm, proceeded via a concerted bond cleavage process.

3.2 Propylene Sulfide

Propylene sulfide (C_3H_6S) is a derivative of ethylene sulfide. The absorption spectra of propylene sulfide and ethylene sulfide show a similar feature near 193 nm, but with different intensity. Five primary dissociation channels were observed from photodissociation of propylene sulfide at 193 nm excitation, shown as the following:

$C_3H_6S + h\nu_{193nm} \rightarrow S(^1D) + C_3H_6$ (propylene) $\Delta H_{rxn} = -53.2$ kcal/mol **(7)**

$C_3H_6S + h\nu_{193nm} \rightarrow S(^3P) + C_3H_6$ (propylene) $\Delta H_{rxn} = -79.7$ kcal/mol **(8)**

$C_3H_6S + h\nu_{193nm} \rightarrow HS + C_3H_5$ $\Delta H_{rxn} = -75.7$ kcal/mol **(9)**

$C_3H_6S + h\nu_{193nm} \rightarrow H_2S + C_3H_4$ $\Delta H_{rxn} = -110.1$ kcal/mol **(10)**

$C_3H_6S + h\nu_{193nm} \rightarrow CH_3 + C_2H_3S$ $\Delta H_{rxn} = -89.4$ kcal/mol **(11)**

All observed channels are similar to photodissociation of ethylene sulfide at 193 nm except the H atom elimination channel. In this article, we will focus our discussion on the $S + C_3H_6$ channel.

3.2.A. TOF spectra of m/e = 32 (S) and 42 (C_3H_6).

Fig. 8(a) and 8(b) show TOF spectra of m/e = 32 (S) with a probe photon energy of 9.5 eV and the indicated scattering angles. This corresponds to the first excited state $S(^1D)$, since the photon energy used here is below the IP (10.36 eV) of the ground state sulfur $S(^3P)$. A translational energy distribution, $P(E_T)$, shown in Fig. 9 (the solid line) was used to fit the TOF data of Fig. 8(a and b) very well. This distribution corresponds to a channel forming $S(^1D) + C_3H_6$. The maximum translational energy for this channel is derived to be 53 kcal/mol with an average translational energy of 24.1 kcal/mol. In fact, this $P(E_T)$ also includes three components, but is less clear than that of ethylene sulfide. Two peaks are discerned at 31 and 3 kcal/mol, respectively. A shoulder is around at 15 kcal/mol. We also label three distributions as **A**, **B**, and **C** (the dash line) in order to describe their origins conveniently. This multiple component distribution is very similar to our previous study of ethylene sulfide. It should be pointed out that, again, these three $P(E_T)$s are arbitrary somewhat. Again, we associate each distribution with dissociation from different potential energy surfaces, to be discussed later.

Depending on the isomer of mass 42 (C_3H_6), two possible dissociation channels are allowed energetically. They are:

$C_3H_6S + h\nu_{193nm} \rightarrow S(^1D) + C_3H_6$(propene) $\Delta H_{rxn} = -53.2$ kcal/mol **(7a)**

$C_3H_6S + h\nu_{193nm} \rightarrow S(^1D) + C_3H_6$(cyclopropane) $\Delta H_{rxn} = -45.2$ kcal/mol **(7b)**

The heats of formation of propylene sulfide, propene, cyclopropane and $S(^1D)$ are 2.74,[41] 4.78,[27] 12.79,[27] and 92.8 [20] kcal/mol, respectively. In each case, the available energy is 53.2 kcal/mol for reaction (**7a**) and 45.2 kcal/mol for reaction (**7b**), respectively. However, the observed maximum translational energy for this channel is 53 kcal/mol, which is beyond the available energy of the reaction (**7b**). Thus, cyclopropane could be excluded from our study, and C_3H_6 is therefore assigned to propylene. Propylene is a reasonable product, because two weak C-S bonds cleave to form propylene and sulfur with little assiciated geometry change.

The above measurements were repeated at 10.8 eV, and the TOF spectra are shown in Fig. 8(c) and 8(d). Two peaks are clearly observed in the TOF spectra at the scattering angle of 20°. At this probe energy, both excited $S(^1D)$ and ground $S(^3P)$ products contribute. An additional translational energy distribution shown in Fig. 9(b) was used to fit the 10.8 eV data. This $P(E_T)$ corresponds to a process (**8**). The average translational energy is 6.5 kcal/mol with the maximum translational energy extending out to 65 kcal/mol, which within the available energy of reaction (**8**). In the case of ethylene sulfide, however, three peaks were clearly observed at 10.8 eV probe energy with the scattering angle of 20°.

Fig. 10(a) and 10(b) show the TOF spectra of m/e 42, the momentum-matched partner of m/e 32, at the indicated scattering angles and 10.8 eV photon energy. The TOF spectra of m/e 42 were fitted very well using the $P(E_T)$s shown in Fig. 9, with some adjustment of their relative contributions, consistent with the anticipated dependence of the photoionization cross section on internal energy in the product. A low-resolution PIE curve of mass 42 was measured to estimate the internal energy distribution of the fast part and the slow part. Fig. 11(a) and 11(b) show the PIE curve of mass 42 by integrating the fast peak and the slow peak. Two onsets are located to be 9.3 eV and 8.8 eV for the fast and slow part, respectively.

3.2.B. Branching ratio measurements

A similar method as section **3.1.C** was used to measure the branching ratio of $S(^1D):S(^3P)$ from 193 nm photodissociation of propylene sulfide. Thus, measurements of

TOF spectra of m/e 32 were made at 15.0 eV photoionization energy and are shown in Fig. 10(c) and 10(d). These TOF spectra were fitted very well using translational energy distributions of Fig. 9. According to this fit, the branching ratio of $S(^1D):S(^3P)$ is 0.72:0.28.

3.2.C. Dissociation mechanism

The three components of Fig. 9(a) correspond to the $S(^1D) + C_3H_6$ channel. It is very similar to a channel of $S(^1D) + C_2H_4$ from ethylene sulfide photodissociation at 193 nm. Also, the absorption spectra of propylene sulfide and ethylene sulfide show the same feature near 193 nm. Hence, their dissociation mechanisms could have similar nature [18]. Propylene sulfide is excited to $^1A_1$ state, then undergoes three different processes on the singlet potential energy surface (PES): first, direct dissociation on the $^1A_1$ PES forms the fast $S(^1D)$ atoms; secondly, a coupling between $^1A_1$ and $^1B_2$ states gives the middle $S(^1D)$ fragment; the slow $S(^1D)$ comes from internal conversion to the ground state.

The spin-forbidden channel, the $S(^3P) + C_3H_6$ channel, wsa also observed in this system. It is common to observe the spin-forbidden channel from photodissociation of the sulfur compounds mentioned above. On the other hand, dissociation could take place on the ground state by system-crossing to produce the slow $S(^3P)$. The detailed mechanism could be inferred from theoretical investigations.

Excited states of propylene have been studied by different groups [42-44]. The first triplet excited state $1^3A'(\pi\pi^*)$ is about 4.3 eV (99 kcal/mol) above the ground state propylene ($\tilde{X}\ ^1A'$) [42]. The available energies for reaction **7** and **8** are 53.2 and 79.7 kcal/mol, respectively. Hence, the triplet propylene could be excluded from photodissociation of propylene sulfide at 193 nm excitation. On the other hand, the first singlet excited state $1^1A''$ (π 3s) is 6.55 eV (151 kcal/mol) above the ground state [42]. The propylene is therefore formed merely at the ground state in this study. The excited state of propylene cited here is a vertical transition assuming the structure at excited state is unchanged. However, the geometry of excited stated propylene could be distorted. The energy of an adiabatic transition should be lower. To the best of our knowledge, no report has been provided on the adiabatic excitations of propylene.

3.3 Thietane

Thietane (C_3H_6S) is a symmetric four-membered ring. Absorption spectra study showed no distinct peak around 193 nm [19]. Photolysis studies of thietane have been done by several groups [45-50]. Wiebe and Heicklen studied the photolysis of thietane with three photoexcitation wavelengths of 213.9 nm, 228.8 nm, and 253.7 nm [45]. Experiments were done at 25 and 236°C at various pressures and light intensities as well as in the presence of *n*-C_4H_{10}, *i*-C_4H_8, and O_2. In all cases the products were C_2H_4, C_3H_6, and polymer; with O_2 present, SO_2 was also produced; with 253.7 nm radiation, thietane decomposes to C_2H_4 and CH_2S as well as [45]. But Dice and Steer [46] observed C_2H_4 and CH_2S as the only primary dissociation channel with 254 and 313 nm photoexcitation, and the decomposition after excitation to its lowest singlet excited state can be described by initial rupture of a C-S bond and formation of a 1,4-biradical intermediate. However, Dorer and coworkers [49] revisited this system with 214 and 229 nm photolysis, and they thought that thietane undergoes fragmentation to C_2H_4 + CH_2S and a competing reaction to form cyclopropane and sulfur atoms. Energy partitioning indicated that $S(^3P)$ is the atomic fragment when cyclopropane is produced. Furthermore, Dorer et al. presented a mechanism which assumes that, once excited to its $^1B_2$ electronic state, intersystem crossing to the $^3B_2$ state competes with C-S bond rupture that forms the 1,4-diradical intermediate which yields the ring cleavage products. All previous studies have been done in reaction cell via multi-collisions, also reaction products were not detected selectively. Hence, the previous experiments [45,46,49] are not likely to give the primary dissociation products and mechanism unambiguously. We revisited this system with tunable synchrotron radiation as detection. Five primary channels were observed from 193 nm photodissociation of thietane, shown as the following. We will describe the reaction **12** in this article.

$$C_3H_6S + h\nu_{193nm} \rightarrow S\,(^3P) + C_3H_6\ (\text{Propene}) \qquad \Delta H_{rxn} = -91.5\ \text{kcal/mol} \qquad \textbf{(12a)}$$

$$C_3H_6S + h\nu_{193nm} \rightarrow S\,(^1D) + C_3H_6\ (\text{Propene}) \qquad \Delta H_{rxn} = -65.0\ \text{kcal/mol} \qquad \textbf{(12b)}$$

$$C_3H_6S + h\nu_{193nm} \rightarrow HS + C_3H_5 \qquad \Delta H_{rxn} = -88.4\ \text{kcal/mol} \qquad \textbf{(13)}$$

$C_3H_6S + h\nu_{193nm} \rightarrow H_2S + C_3H_4$ (allene) $\Delta H_{rxn} = -122.2$ kcal/mol **(14a)**

$C_3H_6S + h\nu_{193nm} \rightarrow H_2S + C_3H_4$ (propyne) $\Delta H_{rxn} = -123.2$ kcal/mol **(14b)**

$C_3H_6S + h\nu_{193nm} \rightarrow CH_2S + C_2H_4$ $\Delta H_{rxn} = -121.8$ kcal/mol **(15)**

3.3.A. TOF spectra of m/e = 32 (S) and 42 (C_3H_6)

Figure 12(a and b) shows TOF spectra of m/e = 32 (S) at scattering angles of 15° and 30° with a probe photon energy of 9.6 eV, which is below the IP of $S(^3P)$. Hence, the data of m/e = 32 corresponds to the excited state $S(^1D)$. A translational energy distribution, shown in figure 12(c), was used to fit the data very well. The maximum translational energy extends out to 25 kcal/mol with a peak of roughly 5 kcal/mol. However, both reaction **12a** and **12 b** are allowed energetically. It should be easy to distinguish process **12a** and **12b** using the tunable synchrotron radiation as probe light source, if $S(^3P)$ were produced. In fact, we have applied this method successfully to distinguish $S(^3P)$ and $S(^1D)$ successfully in the studies of ethylene sulfide (section **3.1**) and propylene sulfide (section **3.2**) at 193 nm excitation. Figure 13 shows TOF spectra of m/e = 32 (S) at a scattering angle of 15°, but with three different probe photon energies. It is very clear that three TOF spectra are identical with the probe photon energy below and above the IP of $S(^3P)$. This means that the sulfur atoms are formed exclusively in the excited state; no $S(^3P)$ contribution arises from thietane photodissociation at 193 nm. However, photodissociation of most sulfides gives the mixture of $S(^3P)$ and $S(^1D)$: Table 1 lists the branching ratio of $S(^3P)$:$S(^1D)$ from various molecules. Because its outermost $3b_1$ orbital is almost nonbonding the probability of the intersystem crossing is enhanced, even for the simplest sulfides like H_2S [51] and CS_2 [33,36]. But, it is very surprising that the sulfur atom is formed only at the excited state $S(^1D)$ from thietane at 193 nm excitation. One possible explanation is that the dissociation could proceed entirely on an excited potential energy surface of thietane, with two C-S bond ruptures in the concerted manner.

3.3.B. Photoionization efficiency spectra of $S(^1D)$

A low resolution photoionization efficiency spectra (shown in figure 14) of the sole $S(^1D)$ was obtained at the scattering angle of 15°. The onset is about 9.2 eV, which is

close to the IP (9.21 eV) of S(^{1}D). Three obvious peaks are located at 9.6, 10.7, and 11.9 eV, respectively. These peaks include a series of Rydberg transitions, but cannot be discerned in our low resolution measurement. In fact, these peaks are in good agreement with those of S(^{3}P) [30,32], if considering the energy difference of 1.15 eV between S(^{1}D) and S(^{3}P) [20]. Furthermore, two dips at 11.05 and 12.3 eV are the Rydbergs converging limits to higher $^2D^0$ and $^2P^0$ states (see Figure 2), respectively. A high resolution photoionization efficiency spectrum of S(^{1}D) would be of interest for atomic physics

In summary for thietane at 193 nm, tunable synchrotron radiation with PTS gives direct evidence that the sulfur atom is formed solely in the excited state S(^{1}D). The low-resolution photoionization efficiency curve was obtained, and it is comparable to previous measurement of PIE of S(^{3}P).

3.4 Thiophene

In this section, we extend our recent investigations of the photochemistry of complex cyclic molecules to include thiophene, a five-membered sulfur-containing heterocyclic aromatic molecule.

Thiophene is one of the principal sulfur-carrying compounds in fossil fuels, and the study of its photodissociation can provide insights into the properties of sulfur-containing molecules and radicals of importance in fossil fuel combustion [52]. The ultraviolet (UV) photochemistry of thiophene was studied in the gas phase at 213.9, 228.8 and 253.7 nm by Wiebe and Heicklen in the late 1960s using end-product analysis [53]. The primary photofragments inferred from the experiments included C_2H_2, CH_2=C=CH_2, $CH_3C{\equiv}CH$, CS_2, CH_2=CH-C≡CH, and C_2H_2S. Infrared laser multiphoton excitation/dissociation of thiophene was studied by Nayak et al [54]. They proposed a mechanism, which involved breakage of the C-S bond in thiophene to form an unstable 1,5-diradical which further decomposed via different channels. Krishnamachari and Venkitachalam observed a transient absorption spectrum in the region 377 to 417 nm following flash photolysis of thiophene [55]. They tentatively assigned this absorption to C_4H_3. The first direct examination of primary photoproducts of thiophene at 193 nm was carried out by Myers using photofragment translational spectroscopy, and reported in his thesis work but not

otherwise published [56]. Six primary dissociation channels were identified as discussed below. Ng and co-workers [57] examined the isomeric structures of the primary photoproducts formed in the 193 nm photodissociation of thiophene using photodissociation-photoionization detection of the hydrocarbons and 2 + 1 resonance-enhanced multiphoton ionization (REMPI) detection of the sulfur atom. Only two dissociative channels, $C_2H_2S + C_2H_2$ and $C_4H_4 + S$, were observed in their studies and they found that the S atoms were produced predominantly (≥96%) in the ^3P_J states.

Five primary dissociation channels have been identified, including three closed shell channels and two radical channels, as summarized below.

$$C_4H_4S + h\nu_{193\,nm} \rightarrow C_4H_4 + S(^3P) \qquad \Delta H_{rxn} = -36 \text{ kcal/mol} \qquad \textbf{(16)}$$

$$C_4H_4S + h\nu_{193\,nm} \rightarrow C_2H_2S + C_2H_2 \qquad \Delta H_{rxn} = -82.0 \text{ kcal/mol} \qquad \textbf{(17)}$$

$$C_4H_4S + h\nu_{193\,nm} \rightarrow C_3H_4 + CS \qquad \Delta H_{rxn} = -64.3 \text{ kcal/mol} \qquad \textbf{(18)}$$

$$C_4H_4S + h\nu_{193\,nm} \rightarrow HS + C_4H_3 \qquad \Delta H_{rxn} = -26 \text{ kcal/mol} \qquad \textbf{(19)}$$

$$C_4H_4S + h\nu_{193\,nm} \rightarrow HCS + C_3H_3 \qquad \Delta H_{rxn} = -23 \text{ kcal/mol} \qquad \textbf{(20)}$$

TOF spectra of the C_4H_4 and S fragments measured at different angles and the indicated photon energies are shown in Fig. 15. The contribution of dissociative ionization of larger fragments (C_2H_2S, HCS, CS and HS) to sulfur atom may be excluded since a MgF_2 window was used to cut off high-energy scattered radiation. However, these contributions were observed using electron impact ionization in Myers' study [56]. The TOF spectra of mass 32 and 52 were fitted using the translational energy distribution shown in Fig. 16(a). This $P(E_T)$ fits all measured angles. The $P(E_T)$ is peaked at 4 kcal/mol with an average translational energy of 4.9 kcal/mol. This $P(E_T)$ extends out to about 17 kcal/mol.

Depending on the structure of mass 52 (C_4H_4), three possible dissociation channels are allowed energetically [57]. They are:

$C_4H_4S + h\nu_{193\,nm} \rightarrow CH_2{=}CH\text{-}C{\equiv}CH + S(^3P)$ $\Delta H_{rxn} = -36$ kcal/mol **(16a)**

$C_4H_4S + h\nu_{193\,nm} \rightarrow CH_2{=}C{=}C{=}CH_2 + S(^3P)$ $\Delta H_{rxn} = -26.0$ kcal/mol **(16b)**

$C_4H_4S + h\nu_{193\,nm} \rightarrow$ 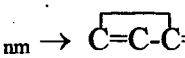 $+ S(^3P)$ $\Delta H_{rxn} = -8.0$ kcal/mol **(16c)**

The analogous channel, $C_4H_4 + O$, was not observed for furan even though above three dissociation channels were energetically allowed [58]. It is likely that the weaker C-S bond contributes to the observation of these channels for thiophene.

The PIE spectrum for C_4H_4 is shown in Fig. 16(b). It is clear that the C_4H_4 fragment is produced predominantly as vinyl acetylene ($H_2C{=}CH\text{-}C{\equiv}CH$). Our assignment is based upon the following considerations. The onset is 9.40 eV labeled by an arrow and is very close to the ionization potential (IP) of vinyl acetylene (9.58 eV) [59]. IP for 1,2,3-butatriene ($CH_2{=}C{=}C{=}CH_2$) and methylenecyclopropene ($C{=}C\text{-}C{=}CH_2$) are 0.25 eV and 1.25 eV lower than the observed onset, respectively. The latter is thus ruled out as a major contributor to the m/e 52 product. The formation of 1,2,3-butatriene (process **16b**) is not excluded by our results, but energetic considerations suggest that **16a** is likely to dominate. Finally, the PIE curve drops down slowly at the region of 9.5 to 9.0 eV. The C_4H_4 fragment likely carries some internal energy, causing the observed threshold to shift toward low energies, although not to the full extent of the average internal energy of 31 kcal/mol (1.34 eV). This is consistent with red-shift of the onset shown in the PIE curve of the C_4H_4 fragment. These conclusions are in good agreement with previous studies [57].

Angular distribution measurements for this channel yielded an isotropic product angular distribution (i.e. $\beta = 0$), implying that the dissociation process takes place on a time scale longer than several molecular rotation periods. This channel likely occurs on the ground potential energy surface.

Since the first excited S (^1D) state lies 26.52 kcal/mol above the ground (^3P) state [20], S (^1D) can be also formed together with vinyl acetylene in process **16a**. Some evidence for excited S (^1D) was observed in this study: that is, S atom product appearing below the IP for S(^3P). However, this product was found at translational energies only accessible with multiphoton excitation, leading us to conclude that it is not a product of single photon dissociation of thiophene.

In summary, the branching ratios of $S(^3P):S(^1D)$ for ethylene sulfide, propylene sulfide, thietane, and thiophene at 193 nm excitation are 0.59:0.41, 0.28:0.72, 0:1.0, and 1.0:0, respectively. These branching ratios likely reflect the strength of the couplings between the initially prepared excited state surface and other surfaces that may play a role in the dissociation. Detailed theoretical calculation would be of great interest to help explain the change of the branchings among these cyclic sulfides.

4. Conclusion

Four cyclic sulfides: ethylene sulfide (C_2H_4S), propylene sulfide (C_3H_6S), thietane (C_3H_6S), and thiophene (C_4H_4S), have been studied using 193 nm photofragmental translational spectroscopy probed via the tunable synchrotron radiation. Experiments show that the photoproducts can be detected selectively. Ethylene sulfide and propylene sulfide show the similar dissociation channels and mechanisms. However, only the excited state $S(^1D)$ was produced from photodissociation of thietane, and only the ground state $S(^3P)$ from photodissociation of thiophene. Dissociation mechanisms for four different cyclic sulfides have been discussed as well as.

Acknowledgments

The authors would like to thank Dr. Osman Sorkhabi, Professor W. -K. Li, Professor D. M. Neumark, Professor L. S. Sheng, and Professor. T. Baer for their contributions to these studies. This work was supported by the Director, Office of Science, Office of Basic Energy Sciences, Chemical Sciences Division of the US Department of Energy under contracts No. DE-AC03-76SF00098 (LBNL) and DE-AC02-98CH1086 (BNL). The Advanced Light Source is supported by the Director, Office of Science, Office of Basic Energy Sciences, Materials Sciences Division of the US Department of Energy, under the same contract.

References:

1 G. E. Busch and K. R. Wilson, *J. Chem. Phys.* **56,** 3626 (1972).

2 G. E. Busch and K. R. Wilson, *J. Chem. Phys.* **56,** 3638 (1972).

3 G. E. Busch and K. R. Wilson, *J. Chem. Phys.* **56,** 3655 (1972).

4 L. J. Butler and D. M. Neumark, *J. Phys. Chem.* **100,** 12801 (1996).

5 P. L. Houston, *J. Phys. Chem.* **100,** 12757 (1996).

6 A. G. Suits, in *Chemical Applications of Synchrotron Radiation*, edited by T. K. Sham (World Scientific, Singapore, 1999).

7 L. J. Butler, *Annu. Rev. Phys. Chem.* **49,** 125 (1998).

8 D. A. Blank, Ph.D. Thesis, University of California, Berkeley, 1997.

9 X. Yang, D. A. Blank, J. Lin, P. A. Heimann, A. M. Wodtke, Y. T. Lee, and A. G. Suits, in *Synchrotorn Radiation Techniques in Industrial, and Materials Science*, edited by D. A. . (Plenum Press, New YorK, 1996), pp. 119.

10 F. Qi, O. Sorkhabi, A. G. Suits, S.-H. Chien, and W.-K. Li, *J. Am. Chem. Soc.* , (in press) (2000).

11 X. Yang, J. Lin, Y. T. Lee, D. A. Blank, A. G. Suits, and A. M. Wodtke, *Rev. Sci. Instrum.* **68,** 3317-3326 (1997).

12 T. K. Minton, P. Felder, R. J. Brudzynski, and Y. T. Lee, *J. Chem. Phys.* **81,** 1759 (1984).

13 W.-B. Tzeng, H.-M. Yin, W.-Y. Leung, J.-Y. Luo, S. Nourbakhsh, G. D. Flesch, and C. Y. Ng, *J. Chem. Phys.* **88,** 1658 (1988).

14 B.-M. Haas, T. K. Minton, P. Felder, and J. R. Huber, *J. Phys. Chem.* **95,** 5149 (1991).

15 P. A. Heimann, M. Koike, C. W. Hsu, D. Blank, X. M. Yang, A. G. Suits, Y. T. Lee, M. Evans, C. Y. Ng, C. Flaim, and H. A. Padmore, *Rev. Sci. Instrum.* **68,** 1945-1951 (1997).

16 A. G. Suits, P. Heimann, X. M. Yang, M. Evans, C. W. Hsu, K. T. Lu, Y. T. Lee, and A. H. Kung, *Rev. Sci. Instrum.* **66,** 4841-4844 (1995).

17 X. Zhao, Ph.D. Thesis, University of California at Berkeley, 1988.

18 L. B. Clark and W. T. Simpson, *J. Chem. Phys.* **43,** 3666 (1965).

19 I. Tokue, A. Hiraya, and K. Shobatake, *J. Chem. Phys.* **91,** 2808 (1989).

20 *Atomic Energy Levels*, Vol. I, edited by C. E. Moore (National Bureau of Standards, Washington, D. C., 1952).

21 P. Felder, E. A. J. Wannenmacher, I. Wiedmer, and J. R. Huber, *J. Phys. Chem.* **96,** 4470-4477 (1992).

22 H. L. Kim, S. Satyapal, P. Brewer, and R. Bersohn, *J. Chem. Phys.* **91,** 1047-1050 (1989).

23 M. W. Chase, Jr., *J. Phys. Chem. Ref. Data* **9,** 1-1951 (1998).

24 B. Gemein and S. D. Peyerimhoff, *J. Phys. Chem.* **100,** 19257-67 (1996).

25 W. Tsang, *Heats of Formation of Organic Free Radicals by Kinetic Methods* (Blackie Academic and Professional, London, 1996).

26 M. Ahmed, D. S. Peterka, and A. G. Suits, *J. Chem. Phys.* **110,** 4248 (1999).

27 D. R. Lide, *Handbook of Chemistry and Physics* (CRC, 1995-1996).

28 J. B. Foresman, M. Head-Gordon, J. A. Pople, and M. J. Frisch, *J. Phys. Chem.* **96,** 135 (1992).

29 D. E. Love and K. D. Jordan, *Chem. Phys. Lett.* **235,** 479-483 (1995).

30 S. T. Gibson, J. P. Greene, B. Ruscic, and J. Berkowitz, *J. Phys. B: At. Mol. Phys.* **19,** 2825 (1986).

31 S. T. Pratt, *Phys. Rev. A* **38,** 1270 (1988).

32 C. T. Chen and F. Robicheaux, *Phys. Rev. A* **50,** 3968 (1994).

33 W. S. McGivern, O. Sorkhabi, A. H. Rizvi, A. G. Suits, and S. W. North, *J. Chem. Phys.* **112,** 5301 (2000).

34 M. J. Frisch, G. W. Trucks, H. B. Schlegel, G. E. Scuseria, M. A. Robb, J. R. Cheeseman, V. G. Zakrzewski, J. Montgomery, J. A., R. E. Stratmann, J. C. Burant, S. Dapprich, J. M. Millam, A. D. Daniels, K. N. Kudin, M. C. Strain, O. Farkas, J. Tomasi, V. Barone, M. Cossi, R. Cammi, B. Mennucci, C. Pomelli, C. Adamo, S. Clifford, J. Ochterski, G. A. Petersson, P. Y. Ayala, Q. Cui, K. Morokuma, D. K.

Malick, A. D. Rabuck, K. Raghavachari, J. B. Foresman, J. Cioslowski, J. V. Ortiz, A. G. Baboul, B. B. Stefanov, G. Liu, A. Liashenko, P. Piskorz, I. Komaromi, R. Gomperts, R. L. Martin, D. J. Fox, T. Keith, M. A. Al-Laham, C. Y. Peng, A. Nanayakkara, C. Gonzalez, M. Challacombe, P. M. W. Gill, B. Johnson, W. Chen, M. W. Wong, J. L. Andres, C. Gonzalez, M. Head-Gordon, E. S. Replogle, and J. A. Pople, , Revision A7 ed. (Gaussian, Inc., Pittsburgh PA, 1998).

35 F. Qi, M. Ahmed, D. S. Peterka, O. Sorkhabi, and A. G. Suits, *J. Chem. Phys.* , unpublished (2000).

36 I. M. Waller and J. W. Hepburn, *J. Chem. Phys.* **87,** 3261-8 (1987).

37 C. S. Effenhauser, P. Felder, and J. R. Huber, *Chem. Phys.* **142,** 311-20 (1990).

38 F. Qi, O. Sorkhabi, A. H. Rizvi, and A. G. Suits, *J. Phys. Chem. A* **103,** 8351 (1999).

39 D. D. Davis, R. B. Klemm, W. Braun, and M. Pilling, *Int. J. Chem. Kinet.* **4,** 383 (1972).

40 F. Wu, X. Chen, and B. R. Weiner, *J. Am. Chem. Soc.* **118,** 8417-8424 (1996).

41 S. Sunner, *Acta Chem. Scand.* **17,** 728 (1963).

42 I. C. Walker, T. M. Abuain, M. H. Palmer, and A. J. Beveridge, *Chem. Phys.* **109,** 269 (1986).

43 C. R. Bowman and W. D. Miller, *J. Chem. Phys.* **42,** 681 (1965).

44 R. Derai and J. Danon, *Chem. Phys. Lett.* **45,** 134 (1977).

45 H. A. Wiebe and J. Heicklen, *photolysis of thietane vapor* **92,** 7031 (1970).

46 D. R. Dice and R. P. Steer, *J. Phys. Chem.* **77,** 434 (1973).

47 G. L. Bendazzoli, G. Gottarelli, and P. Palmieri, *J. Am. Chem. Soc.* **96,** 11 (1974).

48 D. R. Dice and R. P. Steer, *Can. J. Chem.* **53,** 1744 (1975).

49 F. H. Dorer, M. E. Okazaki, and K. E. Salomon, *J. Phys. Chem.* **85,** 2671 (1981).

50 S. Braslavsky and J. Heicklen, *Chem. Rev.* **77,** 473 (1977).

51 C. W. Hsu, C. L. Liao, Z. X. Ma, P. J. H. Tjossem, and C. Y. Ng, *Chemical Physics Letters* **199,** 78-84 (1992).

52 A. Weissberger, E. C. Taylor, and S. Gronowitz, in *The Chemistry of Heterocyclic Compounds*, Vol. 44 (1992).

[53] H. A. Wiebe and J. Heicklen, *Can. J. Chem.* **47,** 2965 (1969).

[54] A. K. Nayak, S. K. Sarkar, R. S. Karve, V. Parthasarathy, K. V. S. Rama Rao, J. P. Mittal, S. L. N. G. Krishnamachari, and T. V. Venkitachalam, *Applied Physics B (Photophysics and Laser Chemistry)* **B48,** 437-43 (1989).

[55] S. L. N. G. Krishnamachari and T. V. Venkitachalam, *Chemical Physics Letters* **55,** 116-18 (1978).

[56] J. D. Myers, Ph.D. Thesis, University of California at berkeley, 1993.

[57] C. W. Hsu, C. L. Liao, Z. X. Ma, and C. Y. Ng, *Journal of Physical Chemistry* **99,** 1760-1767 (1995).

[58] O. Sorkhabi, F. Qi, A. H. Rizvi, and A. G. Suits, *J. Chem. Phys.* **111,** 100 (1999).

[59] S. G. Lias, J. E. Bartmess, J. F. Liebman, J. L. Holmes, R. D. Levin, and W. G. Mallard, *J. Phys. Chem. Ref. Data* **17, Suppl. 1** (1988).

[60] G. Nan, I. Burak, and P. L. Houston, *Photodissociation of OCS at 222 nm. The triplet channel* **209,** 383 (1993).

[61] H. Katayanagi, Y. X. Mo, and T. Suzuki, *Chem. Phys. Lett.* **247,** 571 (1995).

[62] C. W. Hsu, C. L. Liao, Z. X. Ma, P. J. H. Tjossem, and C. Y. Ng, *Journal of Chemical Physics* **97,** 6283 (1992).

Table 1. The Branching Ratio of $S(^3P):S(^1D)$ from Various Sulfides

Species	$S(^3P)/S(^1D)$	Wavelength
H_2S	0.87/0.13 [51]	193 nm
CS_2	0.74/0.26 [36]	193 nm
	0.71/0.29 [13]	193 nm
	0.75/0.25 [33]	193 nm
OCS	0.05/0.95 [60]	222 nm
	0.05/0.95 [61]	223 nm
CH_3S	0.15/0.85 [62]	193 nm
C_2H_4S (ethylene sulfide)	0.59/0.41 [a]	193 nm
C_3H_6S (propylene sulfide)	0.28/0.72 [a]	193 nm
C_3H_6S (thietane)	0.0/1.0 [a]	193 nm
C_4H_4S (thiophene)	1.0/0.0 [a]	193 nm

[a] this work.

Figure Captions

1. Photoabsorption spectra of ethylene sulfide, propylene sulfide, and thietane [adapted from Ref. 18].
2. A schematic energy diagram of the neutral sulfur atom and its ion.
3. TOF spectra of m/e = 32 (S) from 193 nm photodissociation of ethylene sulfide. (a) $\Theta = 20°$, 9.5 eV, and (b) $\Theta = 50°$, 9.5 eV: The open circles are experimental data. The dash lines, the dash-dot lines, and the dot lines are the single channel contribution fits using the translational energy distribution $P(E_T)_A$, $P(E_T)_B$, and $P(E_T)_C$ of Figure 4a, respectively. The solid lines are the overall fits. (c) $\Theta = 20°$, 10.8 eV, and (d) $\Theta = 50°$, 10.8 eV: The open circles are experimental data. The dash lines, the dash-dot lines, and the dot lines are the single channel contribution fits using three translational energy distribution $P(E_T)$s of Figure 4a (the solid line), Figure 4b, and Figure 4c, respectively. The solid line are the overall fits.
4. The translational energy distributions $P(E_T)$s from the S + C_2H_4 channels from 193 nm photodissociation of ethylene sulfide: (a) $S(^1D) + C_2H_4(^1A_g)$, (b) $S(^3P) + C_2H_4(^1A_g)$, and (c) $S(^3P) + C_2H_4(^3B_{1u})$.
5. TOF spectra of m/e 28 and 32 from 193 nm photodissociation of ethylene sulfide. (a) m/e = 28, $\Theta = 20°$, 11.0 eV, and (b) m/e = 28, $\Theta = 20°$, 10.0 eV: The open circles are experimental data. The dash lines, the dash-dot lines, and the dot lines are the single channel contribution fits using the translational energy distributions of Figure 4(a, b, and c). The solid lines are the overall fits. (c) m/e = 32, $\Theta = 20°$, 15.0 eV; and (d) m/e = 32, $\Theta = 50°$, 15.0 eV. The dash lines, the dash-dot lines, and the dot lines are the single channel contribution fits using three translational energy distribution $P(E_T)$s of Figure 4a (the solid line), Figure 4b, and Figure 4c, respectively. The solid lines are the overall fits.
6. Energy diagram showing all observed product channels from 193 nm photodissociation of ethylene sulfide, along with exit barriers estimated roughly from our experimental results.

7. Singlet potential energy profiles for dissociation $C_2H_4S \rightarrow C_2H_4(^1A_g) + S(^1D)$ from 193 nm photodissociation of ethylene sulfide, maintaining C_{2v} symmetry throughout.

8. TOF spectra of m/e = 32 (S) from 193 nm photodissociation of propylene sulfide. (a) $\Theta = 20°$, 9.5 eV, and (b) $\Theta = 40°$, 9.5 eV: The open circles are experimental data. The data was fit using the translational energy distribution of Figure 9a. (c) $\Theta = 20°$, 10.8 eV, and (d) $\Theta = 40°$, 10.8 eV: The open circles are experimental data. The dash lines, and the dot lines are the single channel contribution fits using the translational energy distributions of Figure 9a (the solid line), and Figure 9b, respectively. The solid lines are the overall fits.

9. The translational energy distributions $P(E_T)$s from the S + C_3H_6 channels from 193 nm photodissociation of propylene sulfide: (a) $S(^1D) + C_3H_6$, and (b) $S(^3P) + C_3H_6$.

10. TOF spectra of m/e 42 (C_3H_6) and 32 (S) from 193 nm photodissociation of propylene sulfide. (a) m/e= 42, $\Theta = 15°$, 10.8 eV, and (b) m/e = 42, $\Theta = 30°$, 10.8 eV: The open circles are experimental data. The dash lines, and the dot lines are single channel contribution fits using the translational energy distributions of Figure 9a (three components labeled as **A**, **B**, **C**), and Figure 9b, respectively. The solid lines are the overall fits. (c) m/e = 32, $\Theta = 20°$, 15.0 eV, and (d) m/e = 32, $\Theta = 40°$, 15.0 eV: The open circles are experimental data. The dash lines, and the dot lines are the single channel contribution fits using the translational energy distributions of Figure 9a (the solid line), and Figure 9b, respectively. The solid lines are the overall fits.

11. Photoionization efficiency spectra of m/e = 42 (C_3H_6) from 193 nm photodissociation of propylene sulfide. (a) The integrated fast part, (b) the integrated slow part.

12. TOF spectra of m/e 32 (S) from 193 nm photodissociation of thietane. (a), $\Theta = 15°$, 10.7 eV, and (b) TOF spectra of m/e 32, $\Theta = 30°$, 10.7 eV. For (a) and (b), the open circles are experimental data, the data was fit using a translational energy distribution of Figure 12c. (c) Translational energy distribution for the $S(^1D)$ +

C_3H_6 channel from 193 nm photodissociation of thietane. This distribution fits the data of figure 12a and 12b.

13. TOF spectra of m/e = 32 (S) from 193 nm photodissociation of thietane, recorded at a scattering angle of 15°, but with three different probe photon energies: 9.6 eV (the dash line), 10.0 eV (the dash-dot line), and 10.7 eV (the dot line), respectively.

14. Low resolution photoionization efficiency spectra of the sole $S(^1D)$ at the scattering angle of 15° from photodissociation of thietane at 193 nm excitation.

15. TOF spectra of m/e = 32 (S) and 52 (C_4H_4) from 193 nm photodissociation of thiophene. (a) m/e = 32, Θ = 15°, 10.5 eV, (b) m/e = 52, Θ = 20°, 11.0 eV, and (c) m/e = 52, Θ = 30°, 11.0 eV. The open circles are experimental data. The data were fit using a translational energy distribution shown in Figure 16a.

16. (a) The translation energy distribution $P(E_T)$ for the C_4H_4 + S channel from 193 nm photodissociation of thiophene. The $P(E_T)$ was used to fit the TOF data of Figure 15. (b) Photoionization efficiency spectra of C_4H_4 (m/e = 42) from photodissociation of thiophene at 193 nm excitation.

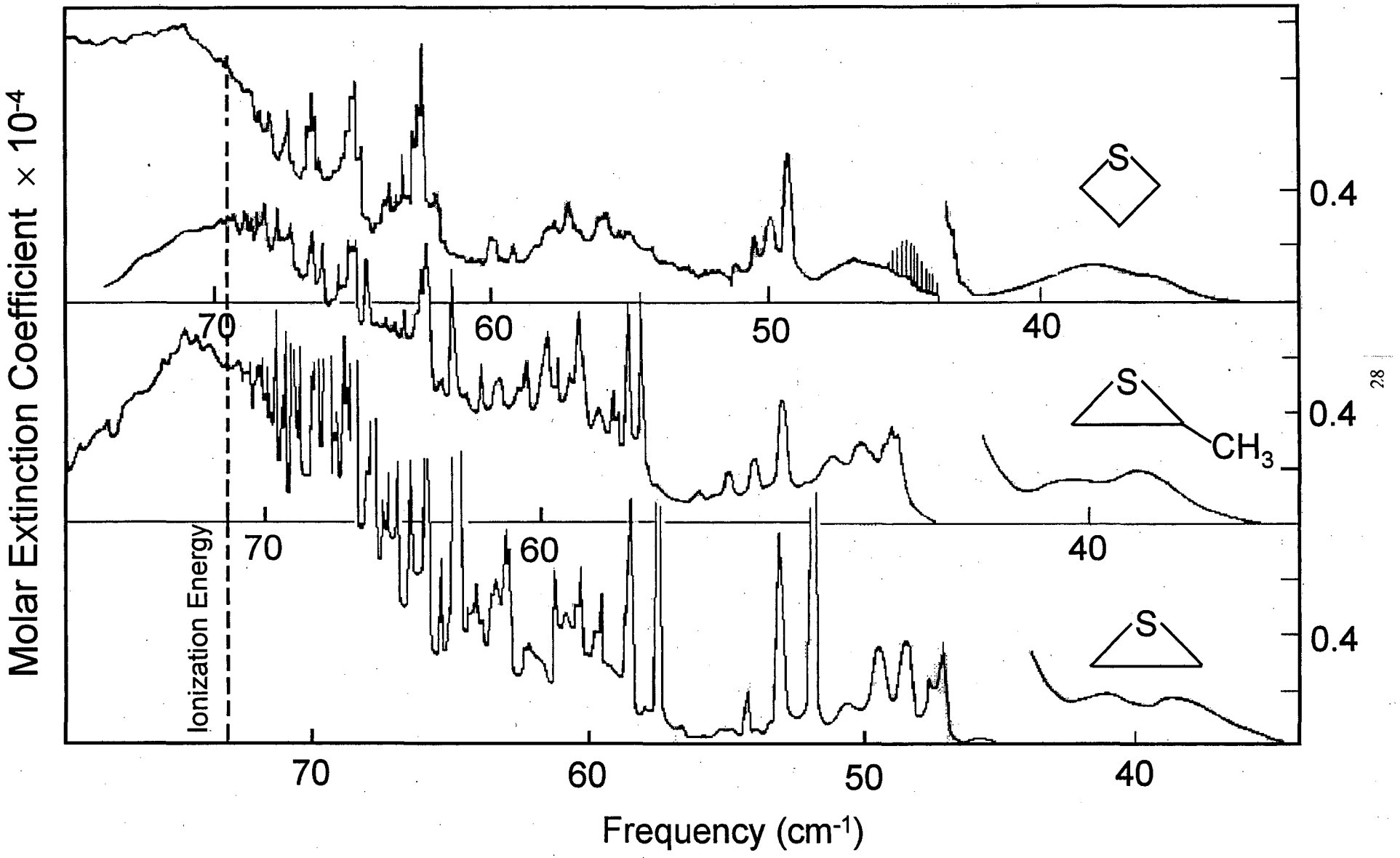
Molar Extinction Coefficient × 10-4
Ionization Energy
70
60
50
40
Frequency (cm-1)
S
S
CH3
S
0.4
0.4
0.4

Suits and Qi: Fig. 2

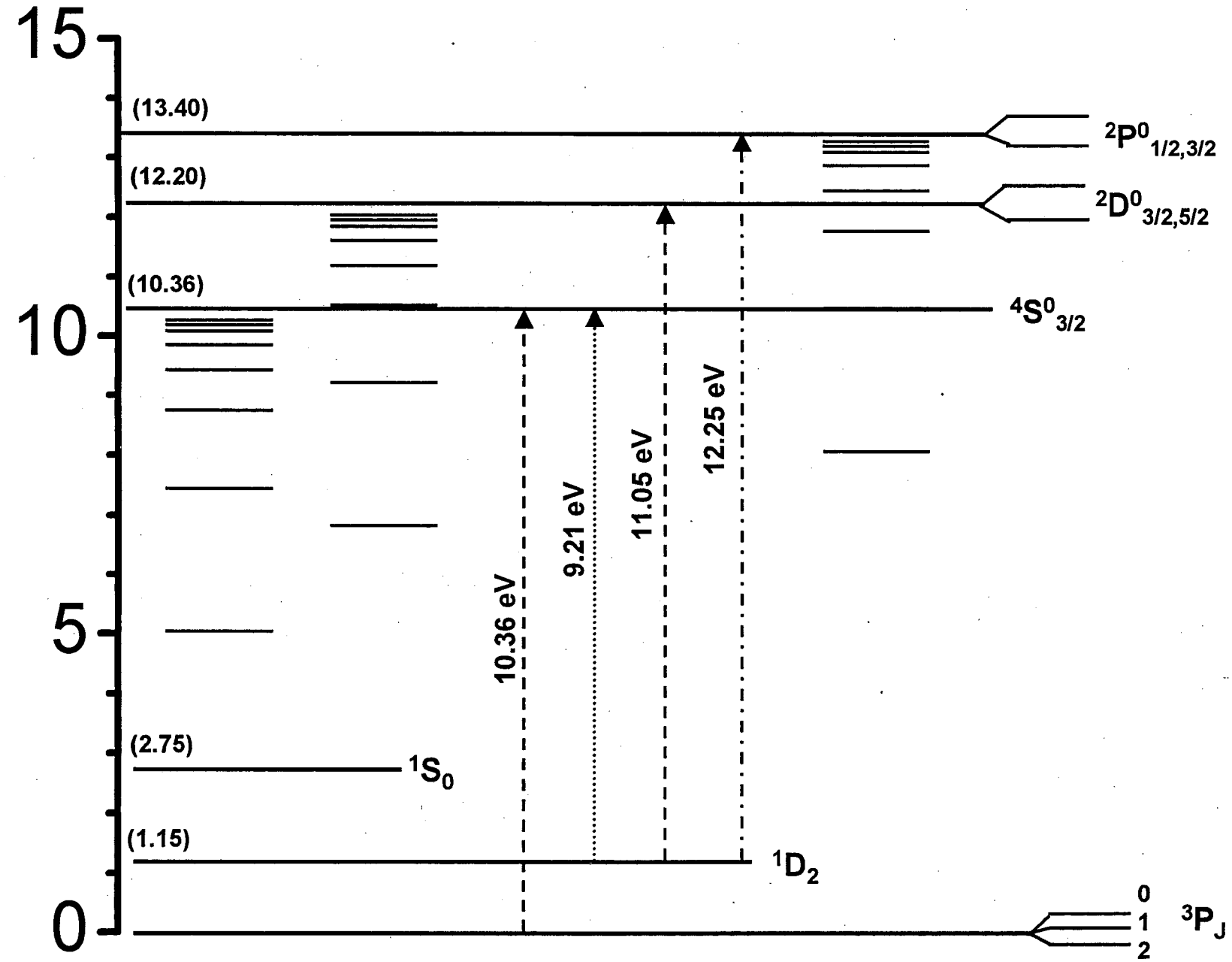

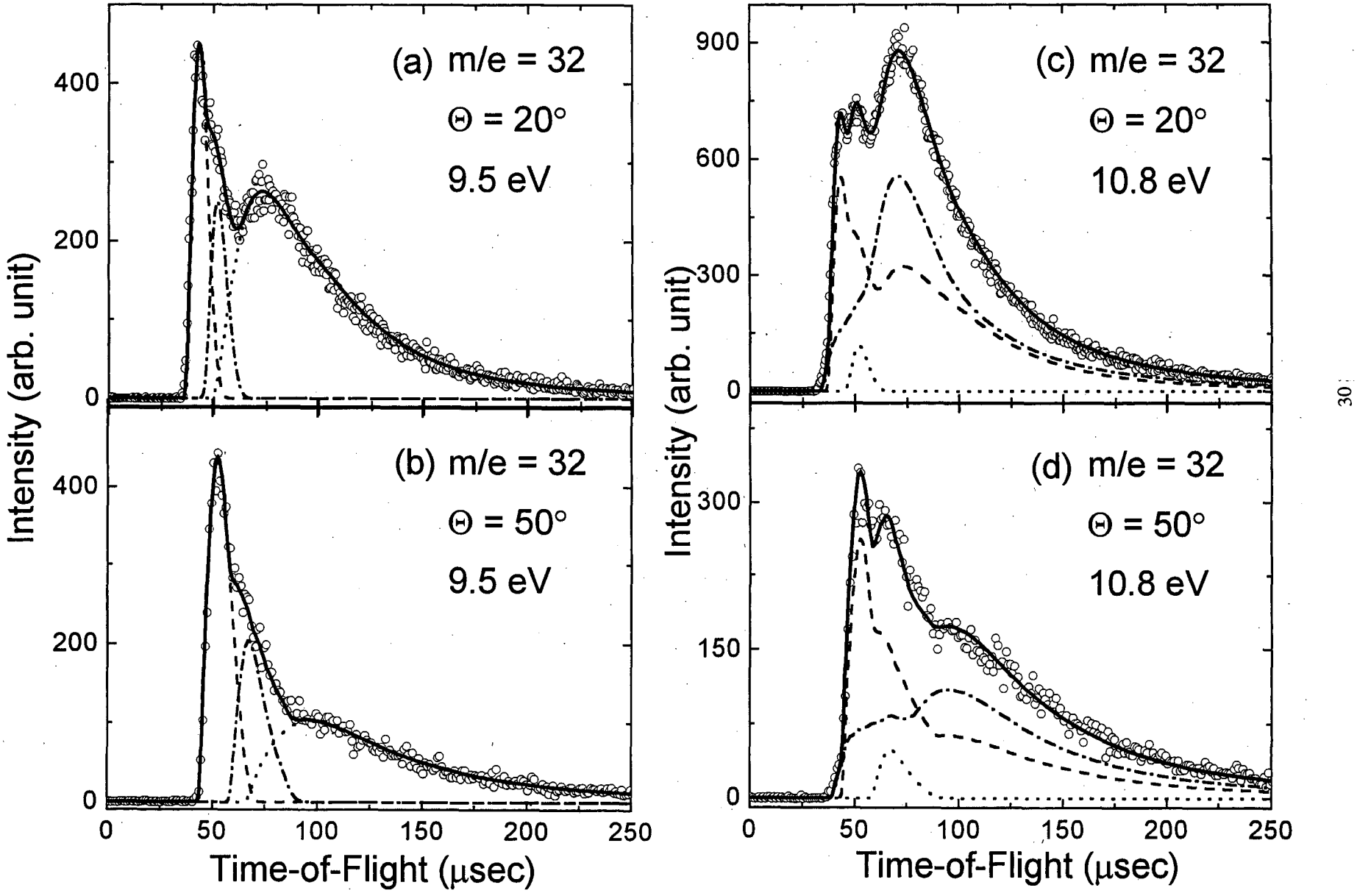
(a) m/e = 32
Θ = 20°
9.5 eV
(b) m/e = 32
Θ = 50°
9.5 eV
(c) m/e = 32
Θ = 20°
10.8 eV
(d) m/e = 32
Θ = 50°
10.8 eV
Intensity (arb. unit)
Time-of-Flight (μsec)
0
50
100
150
200
250
400
200
900
600
300
150

Suits and Qi: Fig. 4

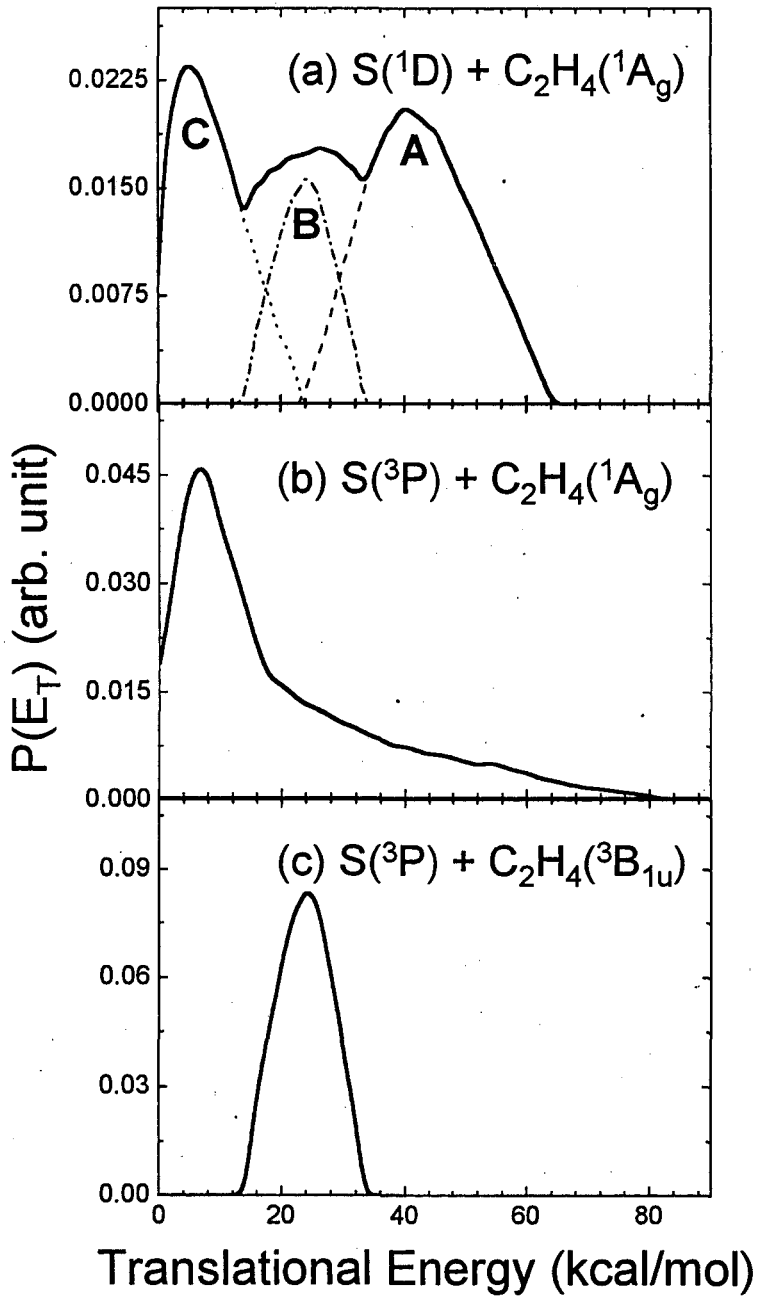

Suits and Qi: Fig. 5

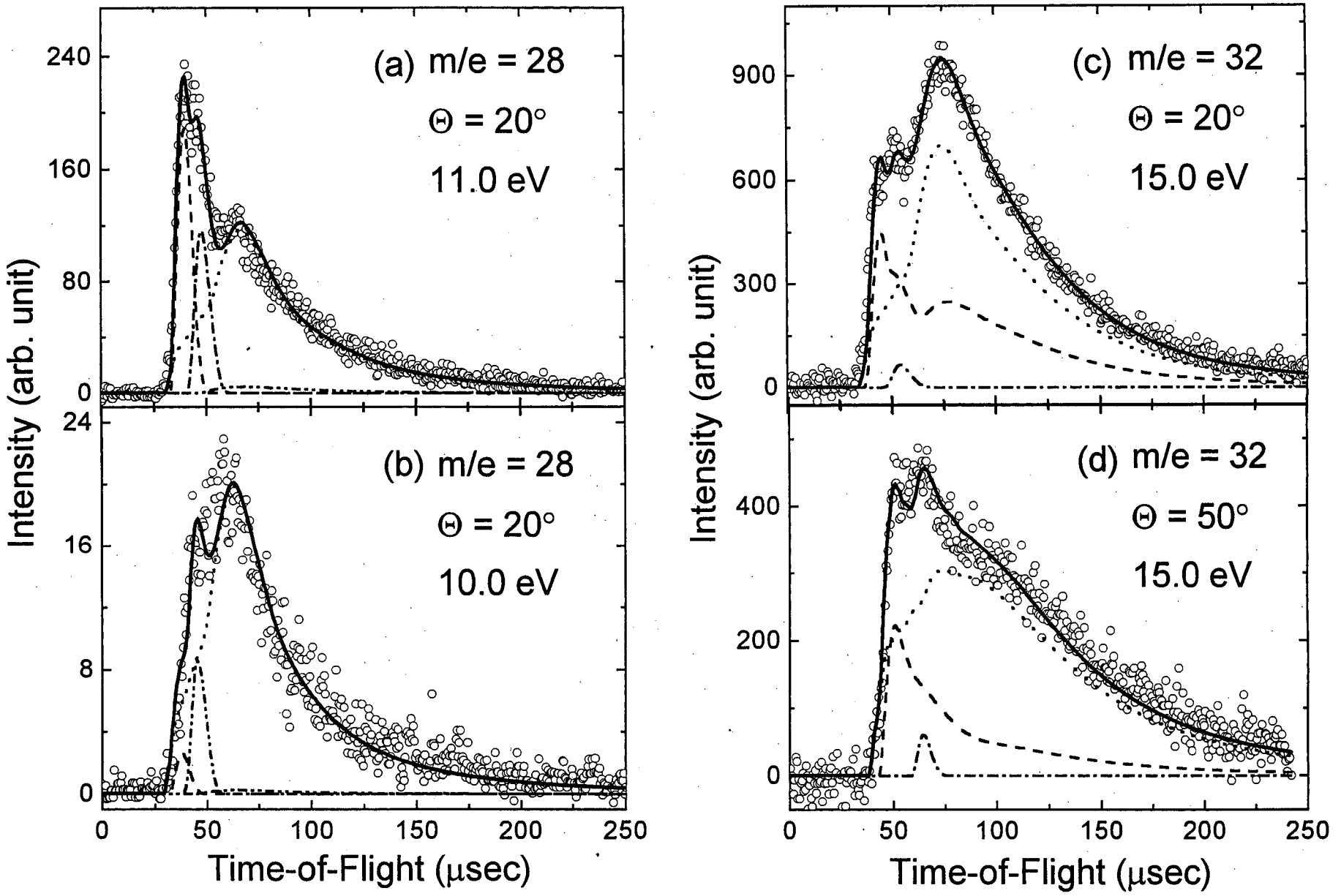

Suits and Qi: Fig. 6

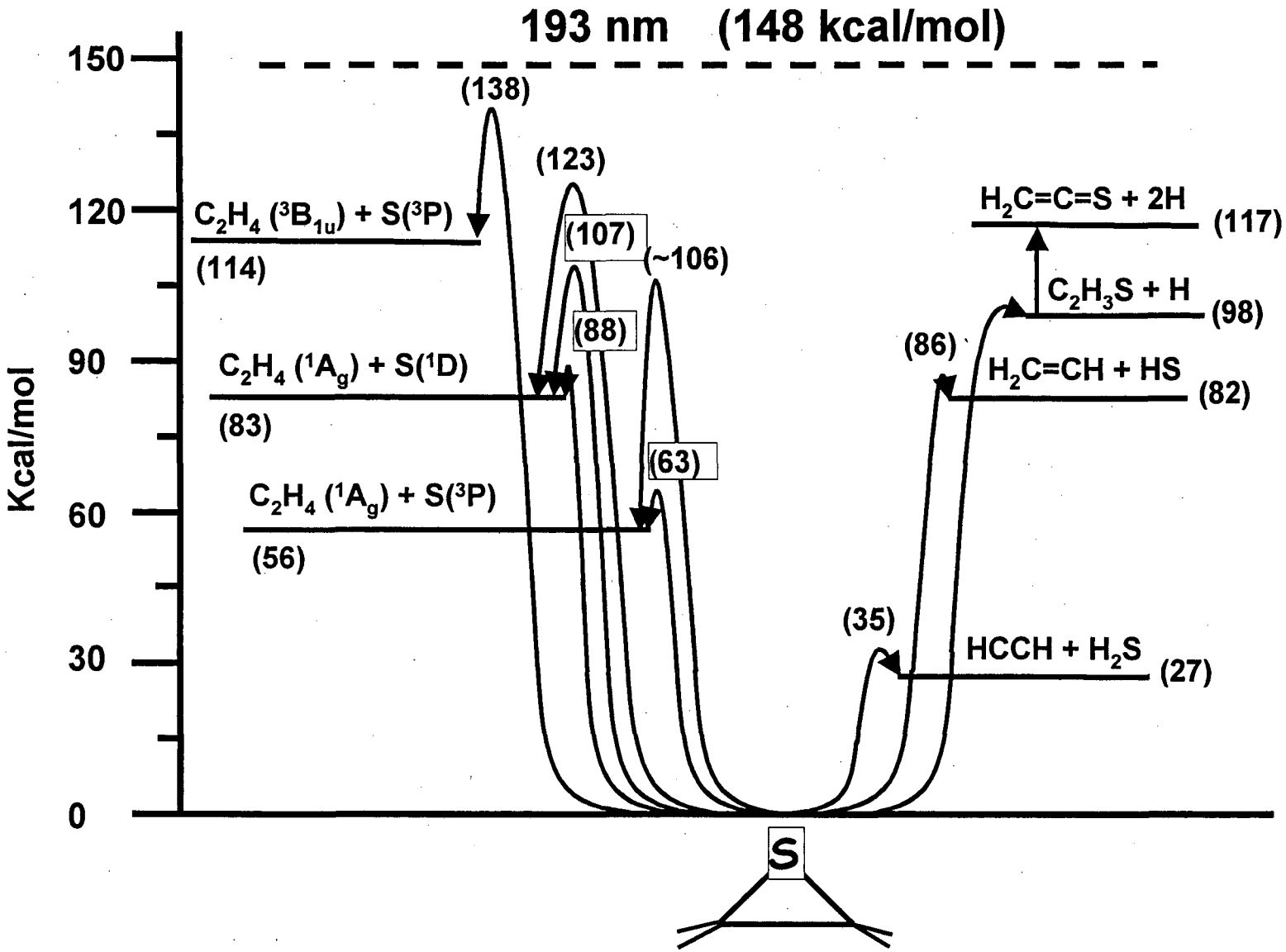

Suits and Qi: Fig. 7

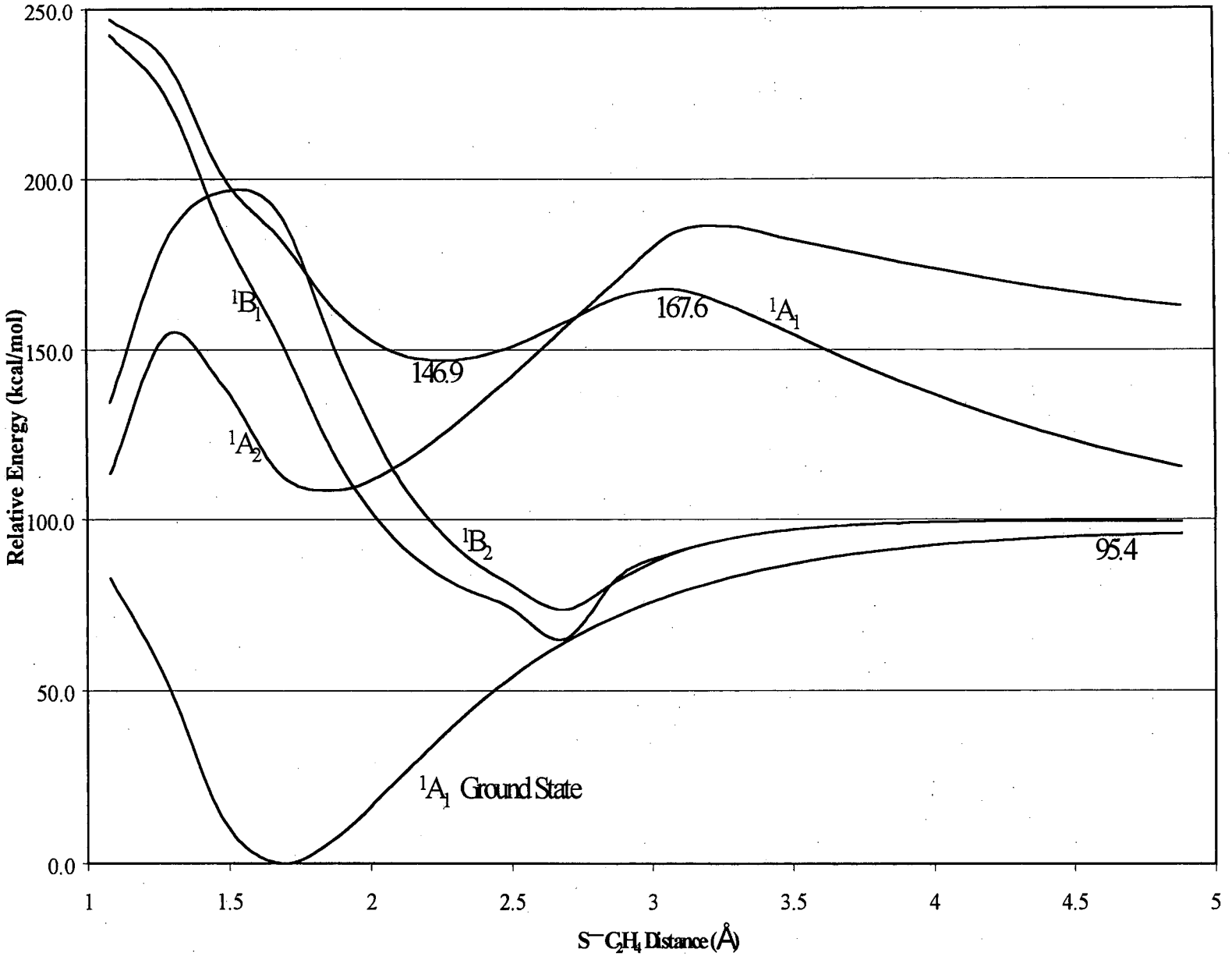

Suits and Qi: Fig. 8

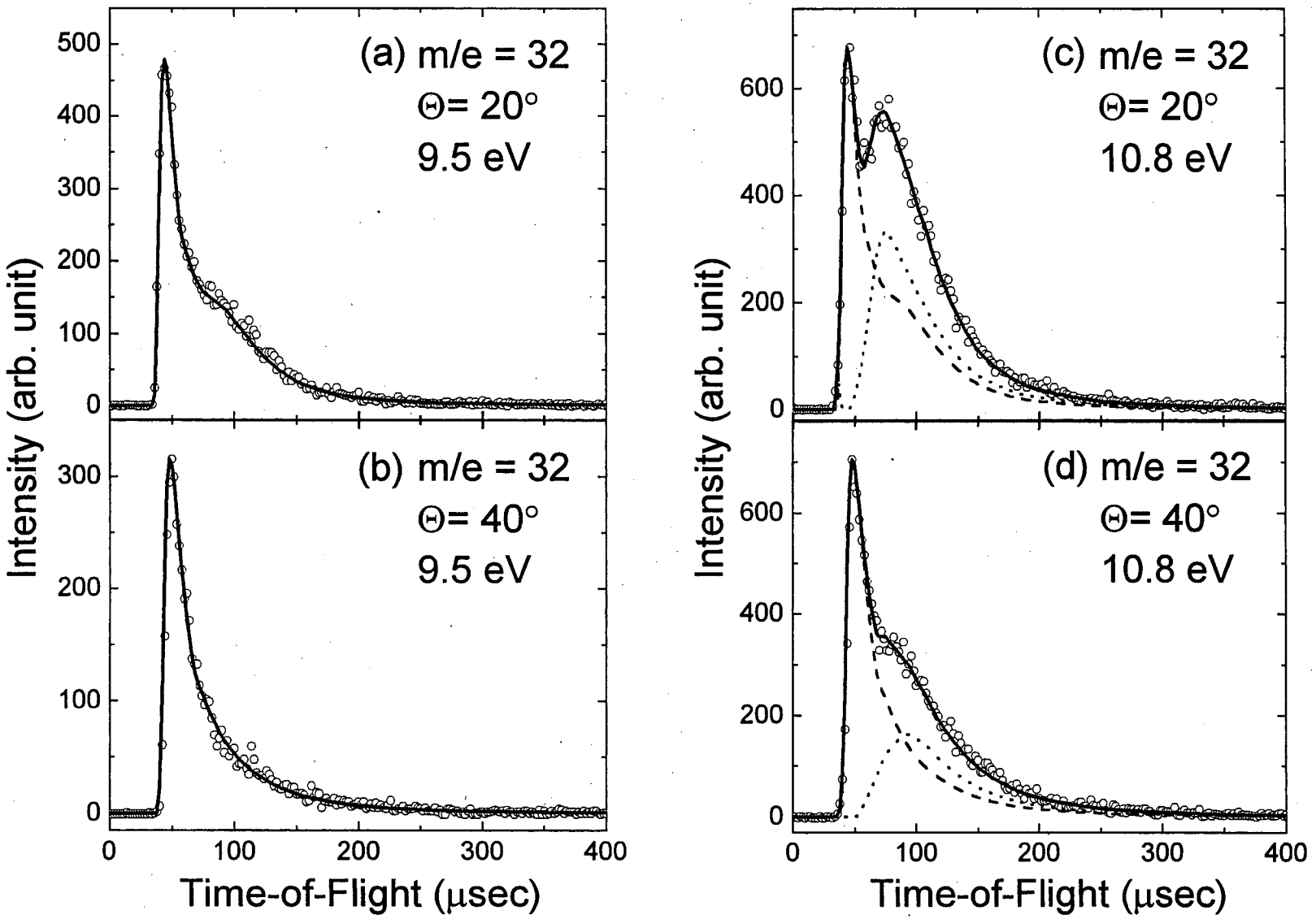

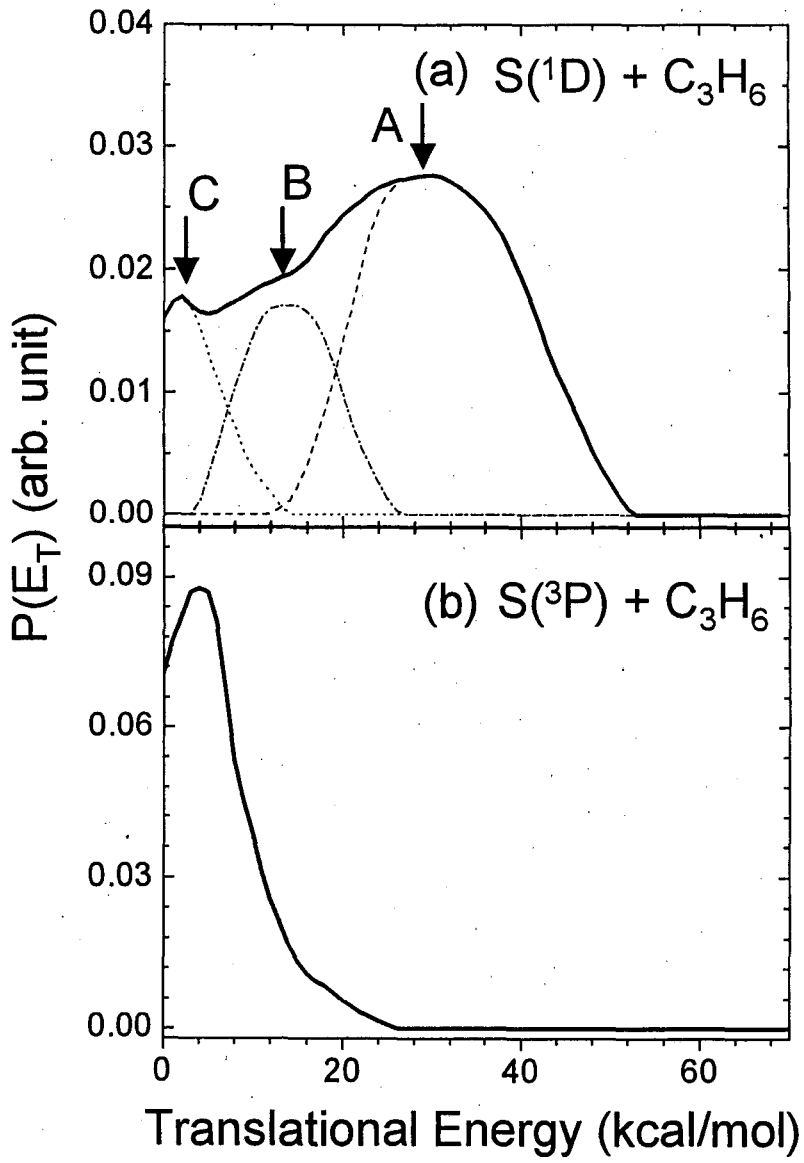
(a) S(1D) + C3H6
A
B
C
(b) S(3P) + C3H6
P(ET) (arb. unit)
Translational Energy (kcal/mol)
0.04
0.03
0.02
0.01
0.00
0.09
0.06
0.03
0.00
0
20
40
60

Suits and Qi: Fig. 10

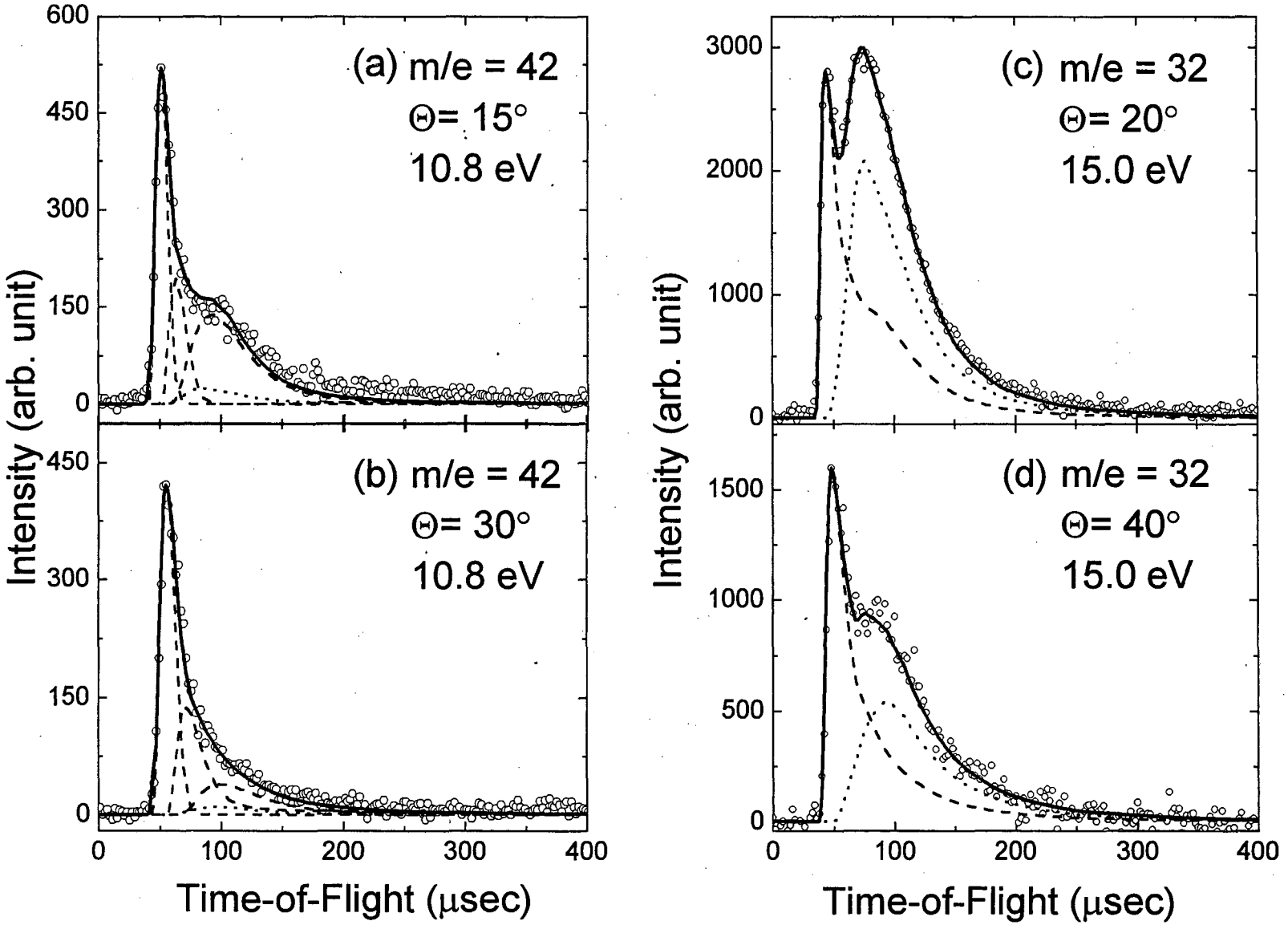

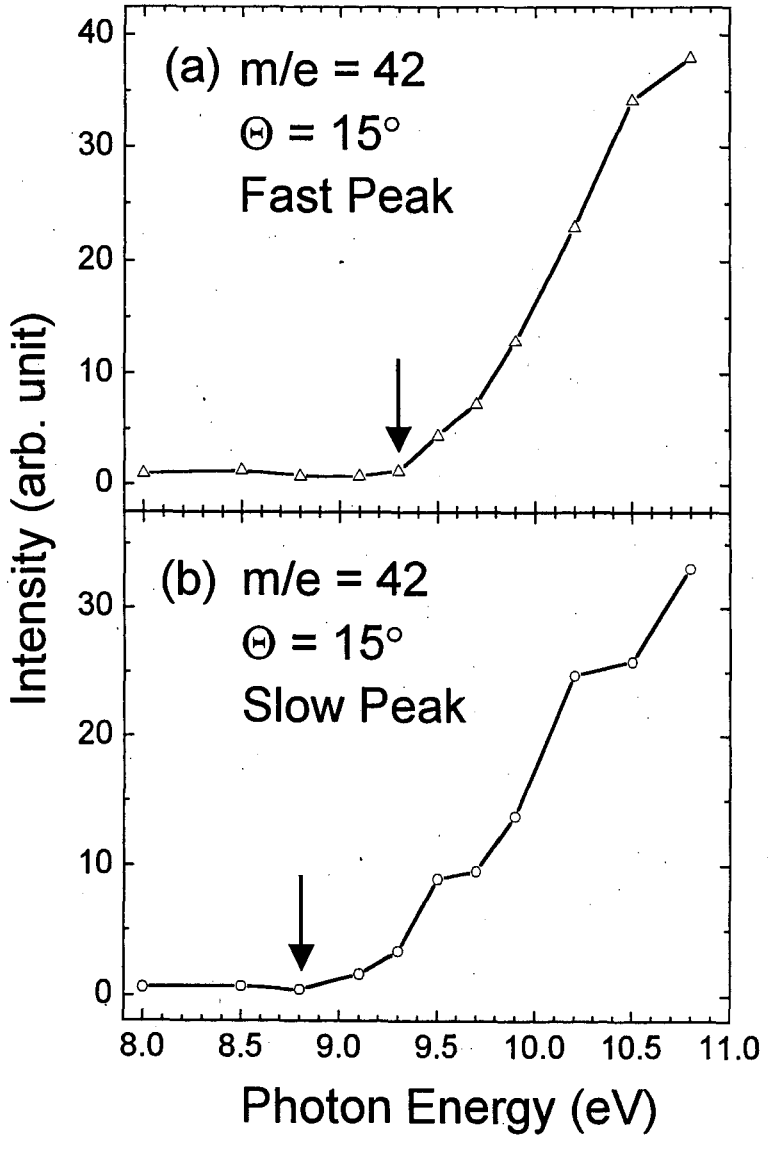
(a) m/e = 42
Θ = 15°
Fast Peak
(b) m/e = 42
Θ = 15°
Slow Peak
Intensity (arb. unit)
Photon Energy (eV)
0
10
20
30
40
8.0
8.5
9.0
9.5
10.0
10.5
11.0

Suits and Qi: Fig. 12

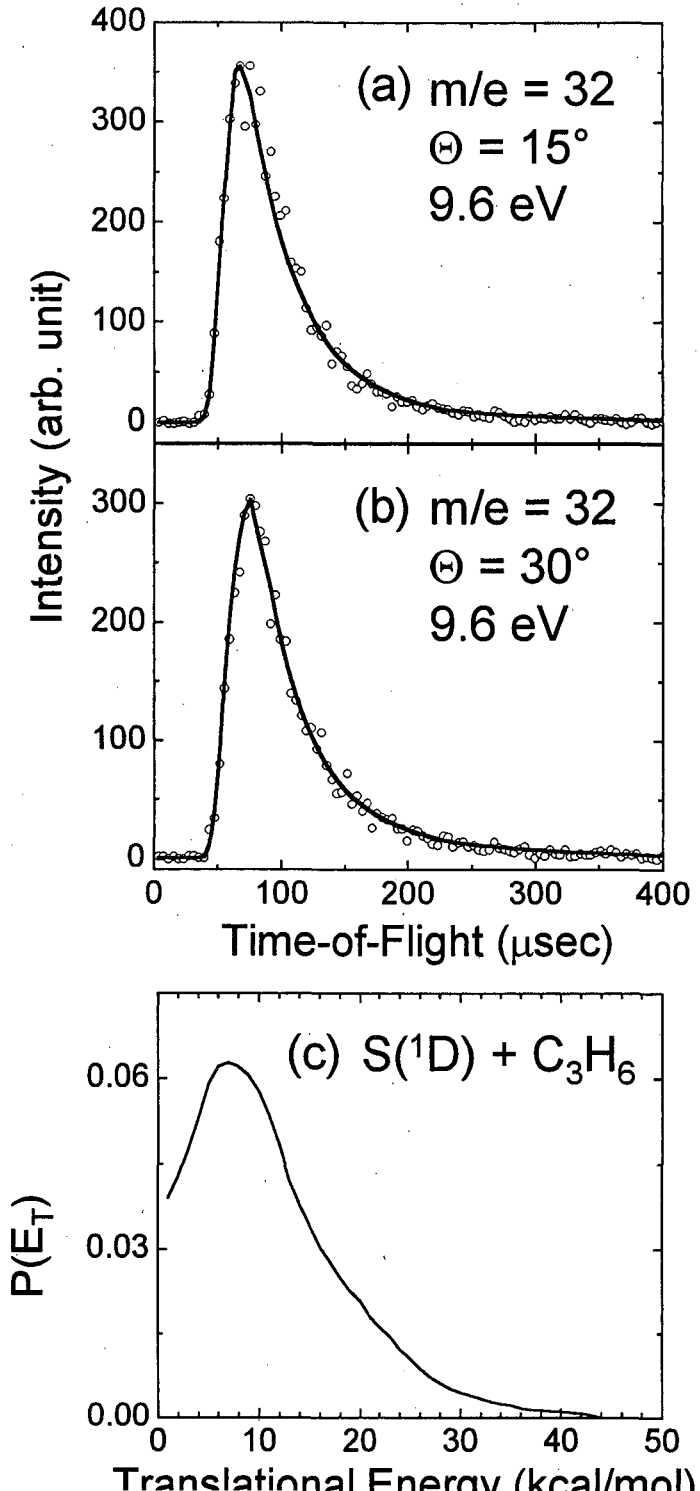

Suits and Qi: Fig. 13

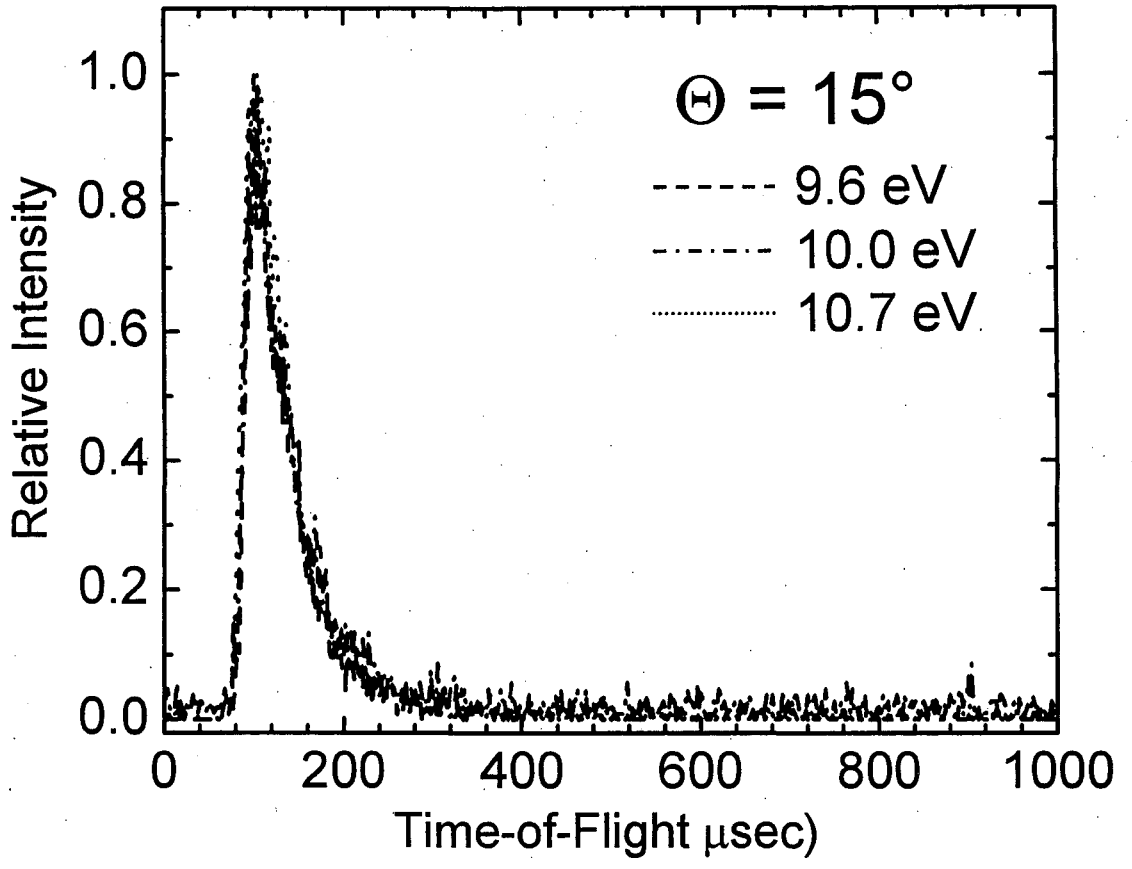

Suits and Qi: Fig. 14

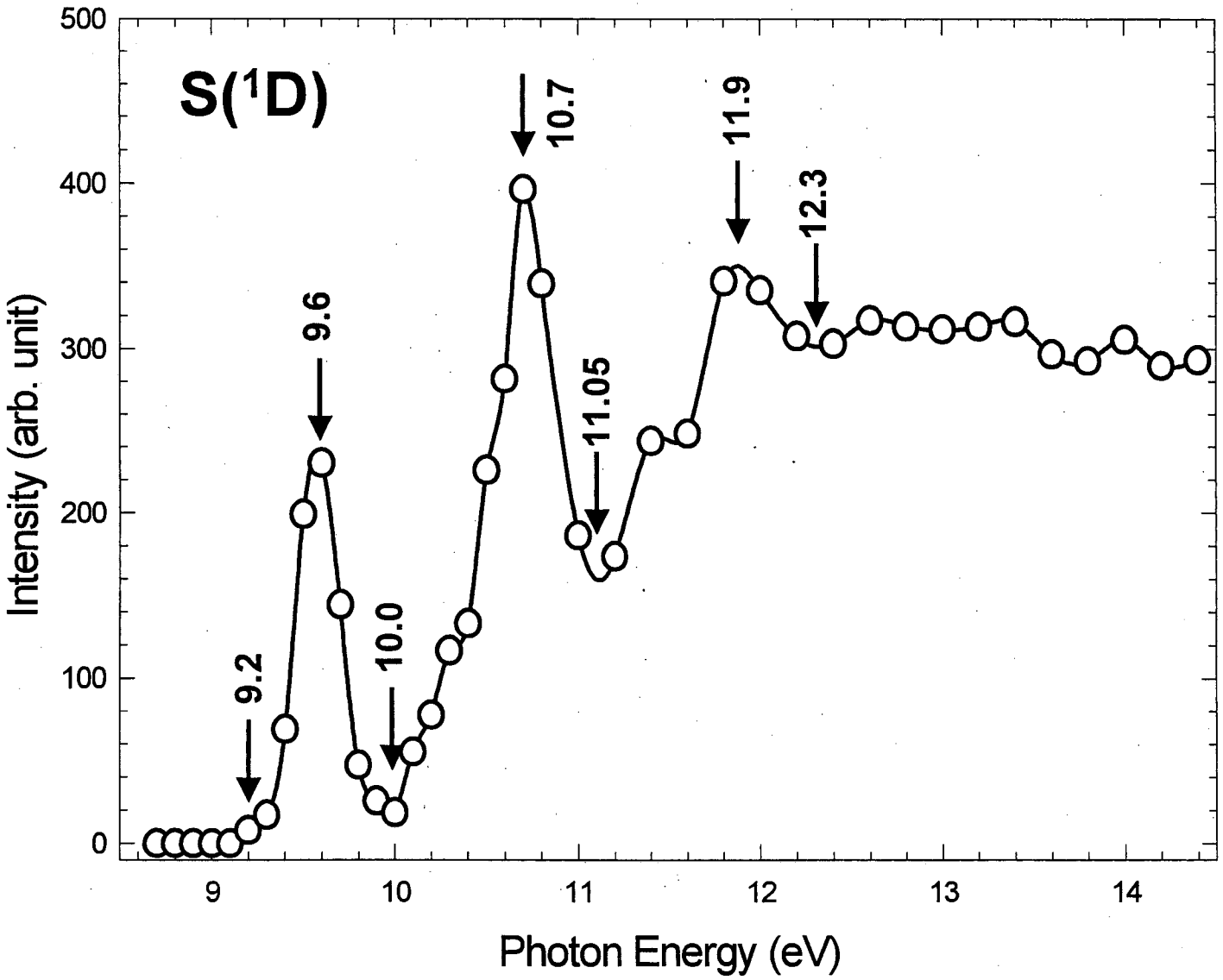

Suits and Qi: Fig. 15

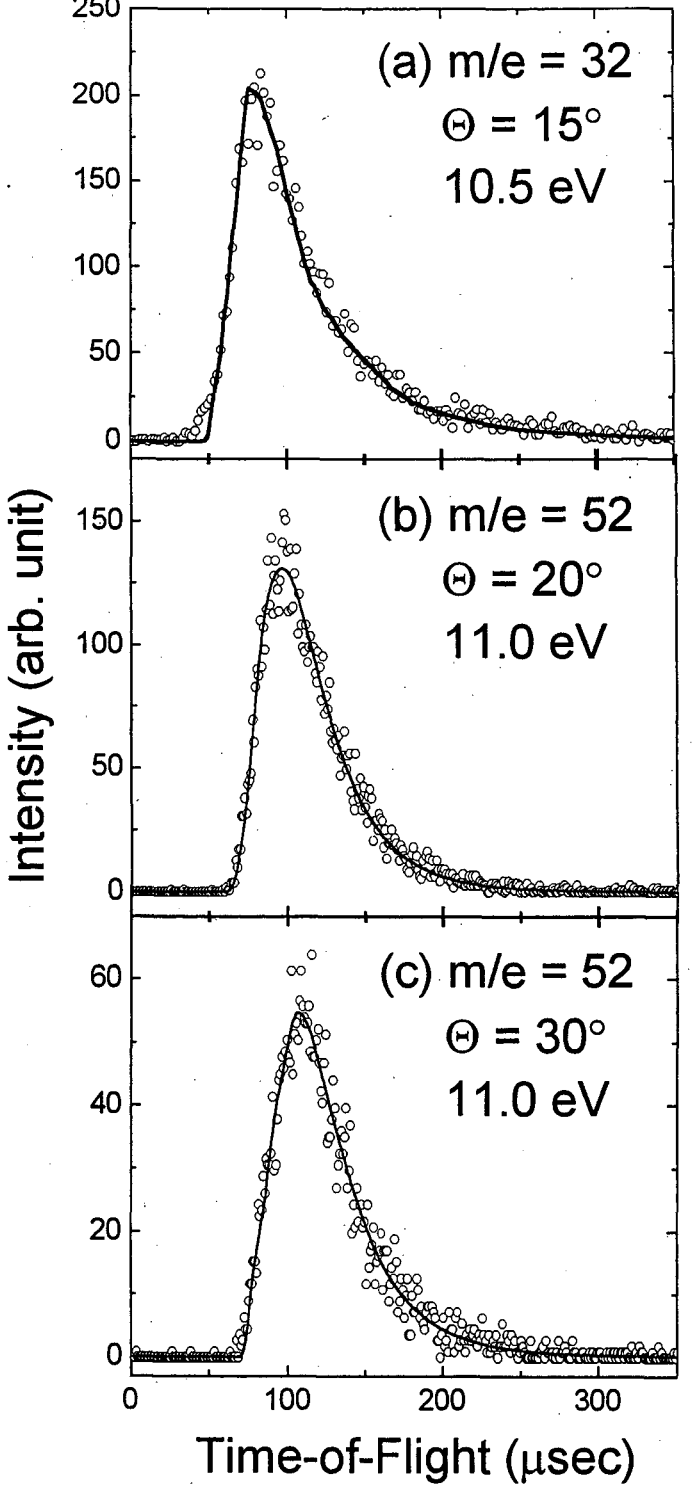

Suits and Qi: Fig. 16

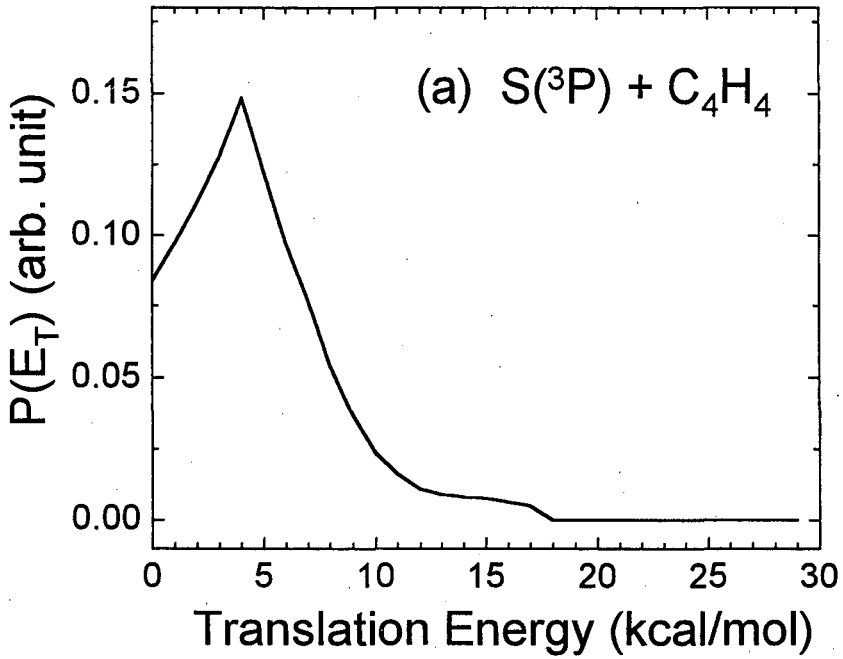

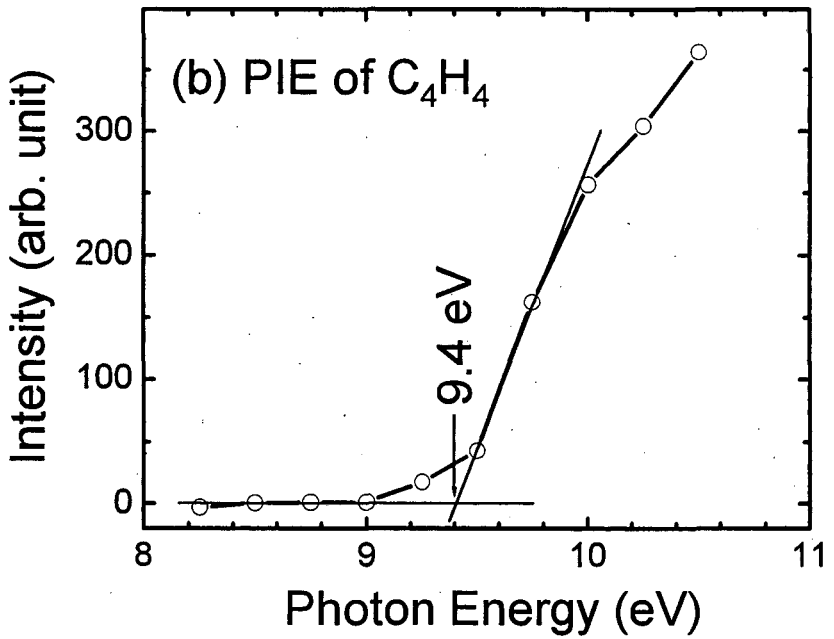

Ernest Orlando Lawrence Berkeley National Laboratory
One Cyclotron Road | Berkeley, California 94720

Prepared for the U.S. Department of Energy under Contract No. DE-AC03-76SF00098